JOURNAL OF GEOPHYSICAL RESEARCH, VOL. 113, B04409, doi:10.1029/2006JB004739, 2008

Extraordinary denudation in the Sichuan Basin: Insights from low-temperature thermochronology adjacent to the eastern margin of the Tibetan Plateau

N. J. Richardson,[1,2] A. L. Densmore,[1,3] D. Seward,[1] A. Fowler,[4,5] M. Wipf,[1,6] M. A. Ellis,[7] Li Yong,[8] and Y. Zhang[8]

Received 6 September 2006; revised 15 February 2007; accepted 31 August 2007; published 17 April 2008.

[1] The eastern margin of the Tibetan Plateau combines very high relief with almost no Tertiary foreland sedimentation and little evidence of Cenozoic tectonic shortening. While river incision and landscape development at the plateau margin have received significant attention over the last decade, little is known about the Cenozoic development of the adjacent Sichuan Basin. Here we assess the Cenozoic thermal history of this basin using detrital apatite fission track (AFT) and (U-Th)/He techniques and establish the presence of an exhumed AFT paleopartial annealing zone across much of the basin. This observation, combined with stratigraphic and borehole sections and inverse modeling of confined apatite fission tracks, indicates that the strata within the basin have undergone accelerated cooling after ~40 Ma, consistent with the widespread erosion of ~1 to 4 km of overlying sedimentary material. This regional-scale erosion is most likely a response to changes in the Yangtze River system draining and removing sediment from the basin. The base-level fall associated with this erosion contributed to a relative increase in relief across the Longmen Shan and may have helped drive Miocene-Recent incision and unloading of the plateau margin.

Citation: Richardson, N. J., A. L. Densmore, D. Seward, A. Fowler, M. Wipf, M. A. Ellis, L. Yong, and Y. Zhang (2008), Extraordinary denudation in the Sichuan Basin: Insights from low-temperature thermochronology adjacent to the eastern margin of the Tibetan Plateau, *J. Geophys. Res.*, *113*, B04409, doi:10.1029/2006JB004739.

1. Introduction

[2] The Tibetan Plateau is the most extensive region of high topography on the face of the Earth and is thus a critical location for answering fundamental questions about the behavior of the lithosphere and the processes that act upon its surface. In particular, the eastern margin of the plateau is a crucial location for testing and understanding the applicability of a number of tectonic models that aim to explain the development of the Tibetan orogen [e.g., *Molnar and Tapponnier*, 1975; *Tapponnier et al.*, 1982; *England and Houseman*, 1986; *Royden et al.*, 1997; *England and Molnar*, 1990] since these models make predictions about the behavior of the lower and upper crust, and by implication, surface processes in this area.

[3] A number of previous studies have focused on obtaining data from the topographically elevated regions along the eastern border of the Tibetan Plateau (Figure 1), with a view to deriving the uplift and denudation history of this geologically enigmatic region [*Kirby et al.*, 2000, 2002, 2003; *Clark et al.*, 2005; *Schoenbohm et al.*, 2004]. The most striking geological conundrum in the area concerns how a major topographic front was created and maintained along the eastern plateau margin with only minor thrust faulting during the Cenozoic [*Burchfiel et al.*, 1995; *Wilson et al.*, 2006]. This is problematic in the framework of traditional tectonic models, especially considering that GPS studies demonstrate that currently only limited convergence (4 ± 2 mm per year) is taking place across the Longmen Shan [*Chen et al.*, 2000; *Zhang et al.*, 2004]. These first-order observations have led to inferences of lower crustal flow being the dominant tectonic mechanism in the area [*Royden et al.*, 1997; *Clark and Royden*, 2000]. This and other models have been assessed to some extent through studies of active faulting (including fault type, rates and magnitudes) [*Burchfiel et al.*, 1995; *Kirby et al.*, 2000, 2003; *Densmore et al.*, 2007] and thermochronology [*Arne et al.*, 1997; *Kirby et al.*, 2002].

[4] Thermochronological studies suggest that this mountainous region, which lies to the west of the Sichuan Basin,

[1]Department of Earth Sciences, Institute of Geology, ETH Zürich, Zürich, Switzerland.
[2]Now at Shell UK Limited, Aberdeen, UK.
[3]Now at Department of Geography, Durham University, Durham, UK.
[4]School of Earth Sciences, University of Melbourne, Melbourne, Victoria, Australia.
[5]Now at AGD Operations, Heathcote, Victoria, Australia.
[6]Now at Geologisch-Paläontologisches Institut, Heidelberg, Germany.
[7]Center for Earthquake Research and Information, University of Memphis, Memphis, Tennessee, USA.
[8]National Key Laboratory of Oil and Gas Reservoir Geology and Exploitation, Chengdu University of Technology, Sichuan, China.

0148-0227/08/2006JB004739$09.00

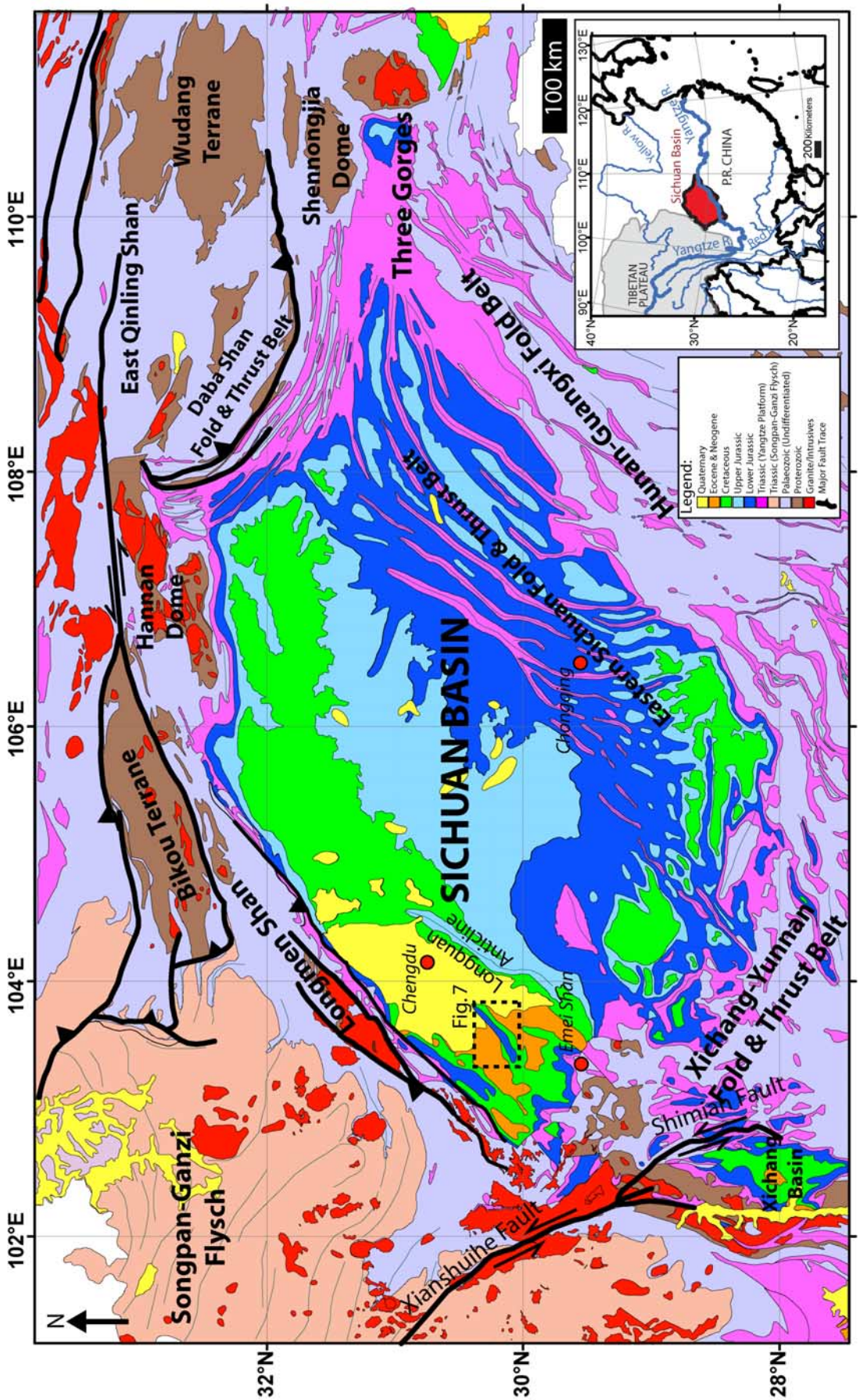

Figure 1. Geological and tectonic map of Sichuan Basin and surrounding regions, compiled from *Ma et al.* [2002]. Note that the outcropping strata within the Sichuan Basin are dominantly of Mesozoic age with the exception of limited Eocene and Quaternary deposits within the westernmost basin. The general outcrop pattern within the basin reflects the exposure of progressively lower stratigraphic levels closer to where the Yangtze River exits the Sichuan Basin near the Three Gorges Region. The dashed box indicates the location of the Xiongpo anticline shown in Figure 7.

may have been elevated since at least the Miocene [*Kirby et al.*, 2002] and since this time, rivers have incised into the plateau area and removed large volumes of sedimentary material [*Kirby et al.*, 2003]. The signal of such major rock uplift and/or denudation should be contained within the Cenozoic sediments of the Sichuan Basin, but since post-Mesozoic strata are missing from much of the basin [*Chen et al.*, 1995; *Burchfiel et al.*, 1995], we have to turn to the offshore sedimentary record to detect this signal, or determine the thermal history of erosion and deposition within the basin using low-temperature thermochronology on the remaining pre-Cenozoic strata.

[5] In this study, we address this latter point through the application of apatite fission track (AFT) and (U-Th)/He thermochronology in order to place constraints on the magnitude and distribution of missing section within the Sichuan Basin, as well as the timing of Cenozoic erosion. We find that the basin experienced widespread erosion of 1–4 km that began sometime after 40 Ma. These results provide first-order constraints on both the topographic development of the eastern Tibetan Plateau and on Cenozoic drainage reorganization in Southeast Asia, in particular the growth and development of the Yangtze River [*Clark et al.*, 2004; *Clift et al.*, 2006].

2. Regional Setting

2.1. Structure and Tectonic Evolution

[6] The present-day Sichuan Basin is a topographically well-defined rhomboid-shaped basin, bounded on all sides by mountains and drained by the Yangtze River and a number of major tributaries (Figure 2). The basement underlying the Sichuan Basin is a component part of the Yangtze Block, which was formed through the Archean and partially reworked in the Proterozoic [*Wang et al.*, 1989; *Zheng et al.*, 2006]. It appears to be structurally distinct from the other parts of the Yangtze Block, based on geophysical evidence, including higher seismic attenuation at depth which corresponds in area with the current topographic low [*Liang et al.*, 2004; *Hearn et al.*, 2004, 2005; *Wang et al.*, 2005; S. Wang et al., S-wave amplitude tomography of China, submitted to *Journal of Geophysical Research*, 2008], strong positive magnetic anomalies under the central basin [*Hsü*, 1989], and magmatic rocks encountered in deep boreholes [*Wang et al.*, 1989].

[7] The Sichuan Basin has experienced relatively little internal deformation, yet it is surrounded by four distinct orogenic belts (Figure 1). To the west lies the Longmen Shan fold and thrust belt, initially formed by the closure of the Songpan-Ganzi ocean basin during the Late Triassic; to the north lies the East Qinling and Daba Shan, a consequence of Triassic collision between the North and South China Blocks; to the south, the Xichang-Yunnan fold and thrust belt, an active region of strike-slip faulting; and to the east lies the Hunan-Guangxi fold belt, a region of intracontinental compression of uncertain Triassic to Cretaceous age. Isopach maps of the Mesozoic strata within the Sichuan Basin (Figure 3) demonstrate that tectonic activity at the margins of the basin shifted its location through time. High topography was initially established in the Longmen Shan during the latter part of the Triassic when the Longmen Shan Foreland Basin developed [*Chen and Wilson*, 1996; *Li et al.*, 2003] (Figure 3a). The locus of deposition then shifted to the northeastern margin of the basin in the Middle Jurassic, probably due to thrusting within the Daba Shan (Figure 1) during continued convergence between the North and South China Blocks (Figure 3b). By Late Jurassic, the main depocenter became "cornered" into the region between the Longmen Shan and Daba Shan margins [*Meng et al.*, 2005] (Figure 3c). The less well studied eastern and southern margins of the Sichuan Basin were probably established as topographically elevated areas relative to the basin by the end of the Cretaceous [*Yan et al.*, 2003], and field evidence suggests that the Sichuan Basin most probably had become an internally drained, or at least sedimentologically closed, basin by this time. The evidence for the development of each of these margins is considered below.

2.1.1. Western Margin: Longmen Shan

[8] The Longmen Shan fold and thrust belt forms the western and most topographically impressive margin of the Sichuan Basin. This zone was an area of significant crustal shortening during the Late Norian-Rhaetian Indosinian orogeny [*Harrowfield and Wilson*, 2005], and the resultant loading of the adjacent region of the Yangtze craton led to its flexural subsidence and the deposition of up to 4 km of clastic sediment in the Longmen Shan Foreland Basin [*Li et al.*, 2003]. This Late Triassic foreland basin is a direct consequence of the closure of the Songpan-Ganzi ocean basin that lay to the west of the Longmen Shan [*Chen and Wilson*, 1996; *Dirks et al.*, 1994; *Burchfiel et al.*, 1995; *Li et al.*, 2003; *Weislogel et al.*, 2006].

[9] Although the climax of accommodation generation within the Longmen Shan Foreland Basin occurred with deposition of the Upper Triassic Xujiahe Group, there is evidence for later fold and thrust activity in the Longmen Shan through the Jurassic and into the Early Cretaceous [*Burchfiel et al.*, 1995; *Arne et al.*, 1997]. These persistent mountain building episodes are reflected not only in a shift of the main sedimentary depocenter to the northeastern corner of the basin [*Meng et al.*, 2005] (Figure 3c), but also in continued metamorphism and crustal deformation within the Longmen Shan and Songpan-Garze regions [*Wallis et al.*, 2003]. The Longmen Shan margin continues to be tectonically active to the present day, with a number of primarily dextral strike-slip faults [*Chen et al.*, 1994; *Kirby et al.*, 2000; *Densmore et al.*, 2007].

[10] As a result of these cyclic episodes of tectonic activity, the Longmen Shan has probably been a region of elevated topography relative to the Sichuan Basin since at least the Late Triassic, as it has been a major source of sediment to the Sichuan Basin since this time. The fact that Upper Triassic marginal foreland basin deposits have yet to be consumed by the eastward propagation of the thrust front into the margin of the basin indicates that the western boundary of the basin has moved minimally since this time [*Li et al.*, 2003].

2.1.2. Northern Margin: East Qinling and Daba Shan

[11] Collision of the North China Block (NCB) and South China Block (SCB) during the Triassic led to the formation of the Qinling-Dabie Orogen [e.g., *Meng and Zhang*, 1999]. The collision initiated at the easternmost end of the orogen, and progressed from east to west, diachronously closing the intervening ocean [*Zhao and Coe*, 1987; *Zhang*, 1997;

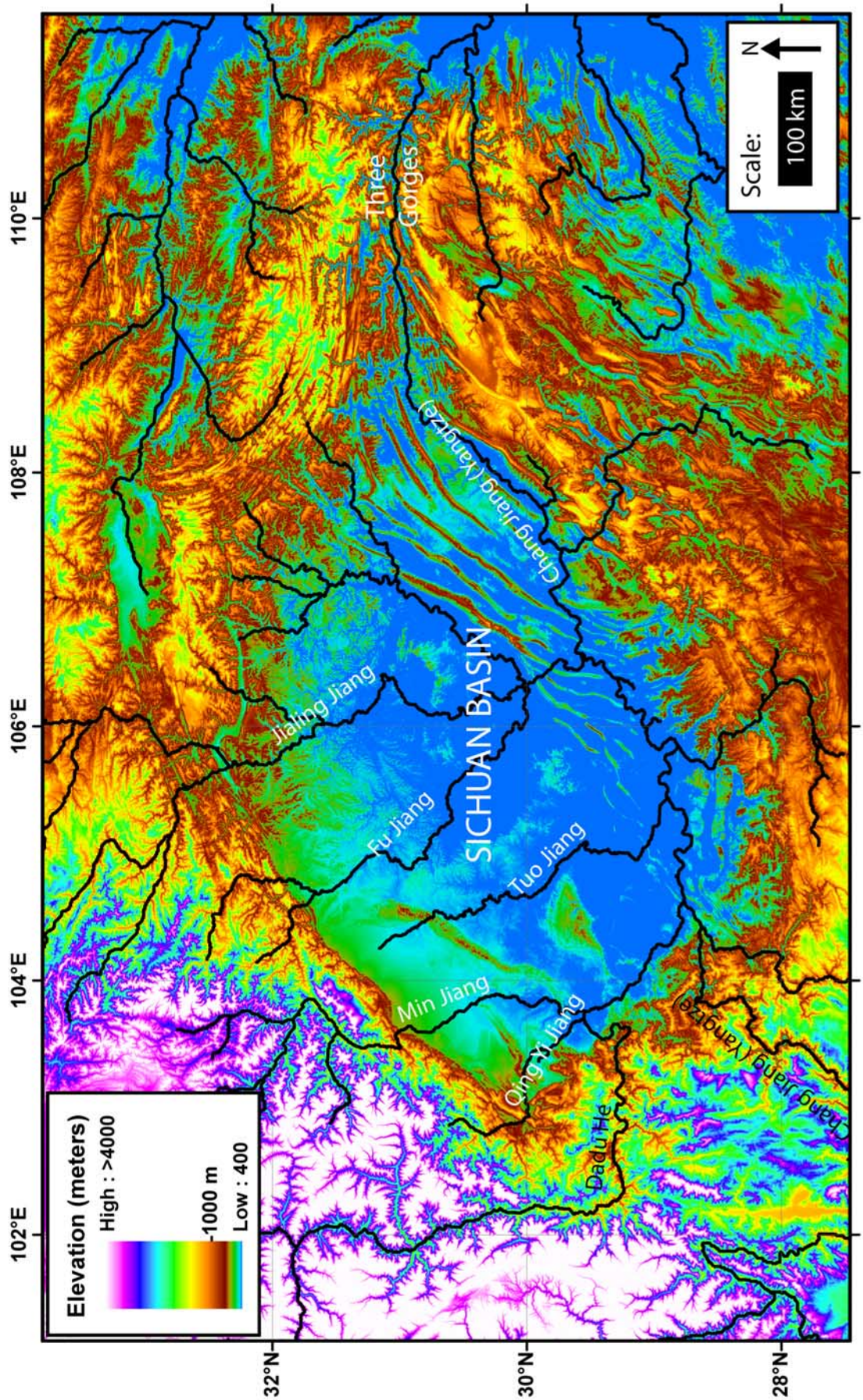

Figure 2. Topography of the Sichuan Basin region derived from SRTM digital elevation model with 3-arc second (~90 m) resolution. Major rivers are shown as black lines.

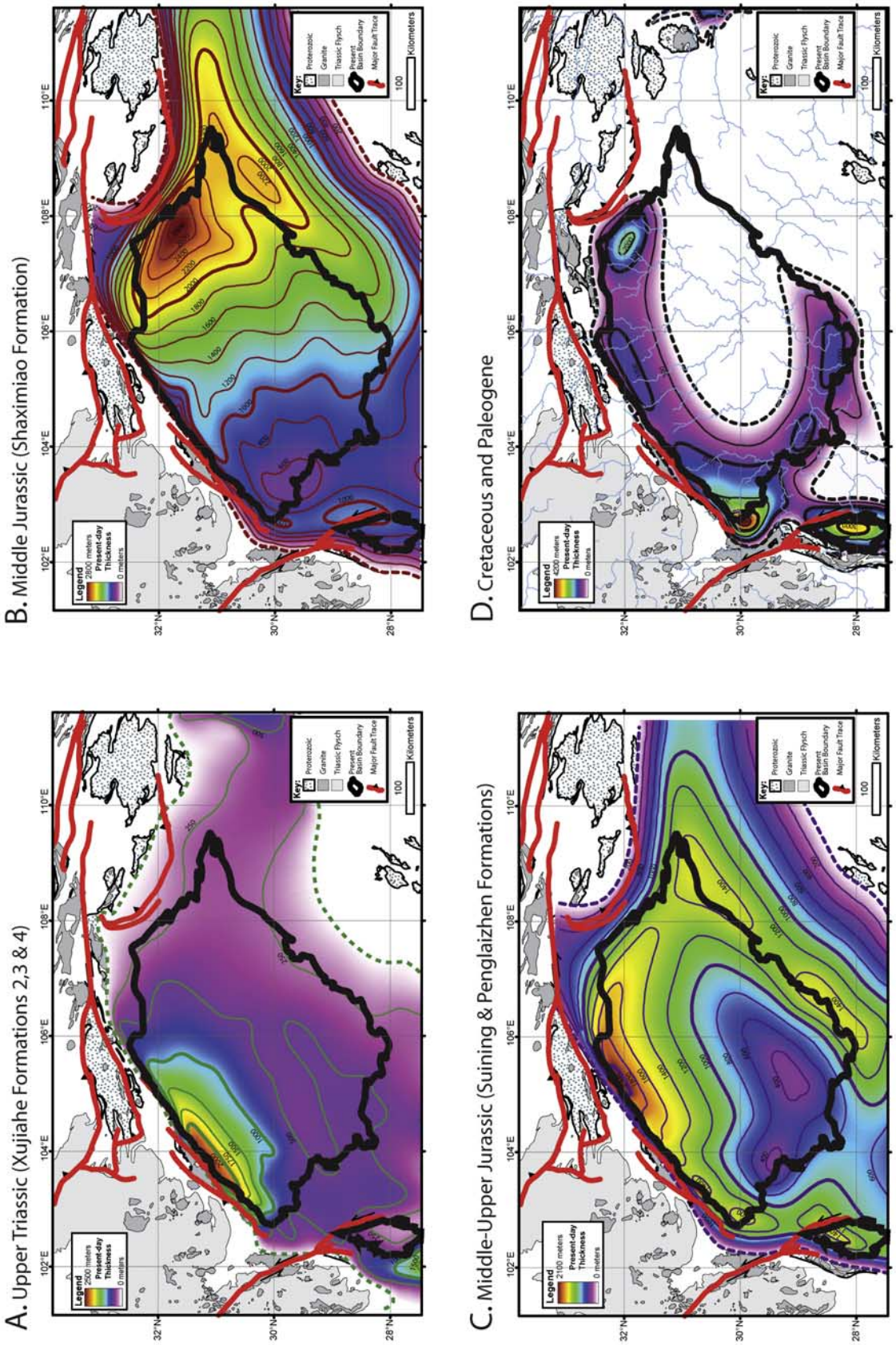

Figure 3. Isopach maps for present-day thicknesses of Mesozoic strata within the Sichuan Basin; data derived from *Petroleum Geology of China* [1987]. Shown are (a) Upper Triassic (Xujiahe Formations 2, 3, and 4); (b) Middle Jurassic (Shaximiao Formation); (c) Middle-Upper Jurassic (Suining and Penglaizhen Formations); (d) Cretaceous and Paleogene. Note that Cretaceous strata are missing over much of the Sichuan Basin and are only observed around the northwestern and southwestern margins of the basin. Heavy black line shows present topographic basin boundary.

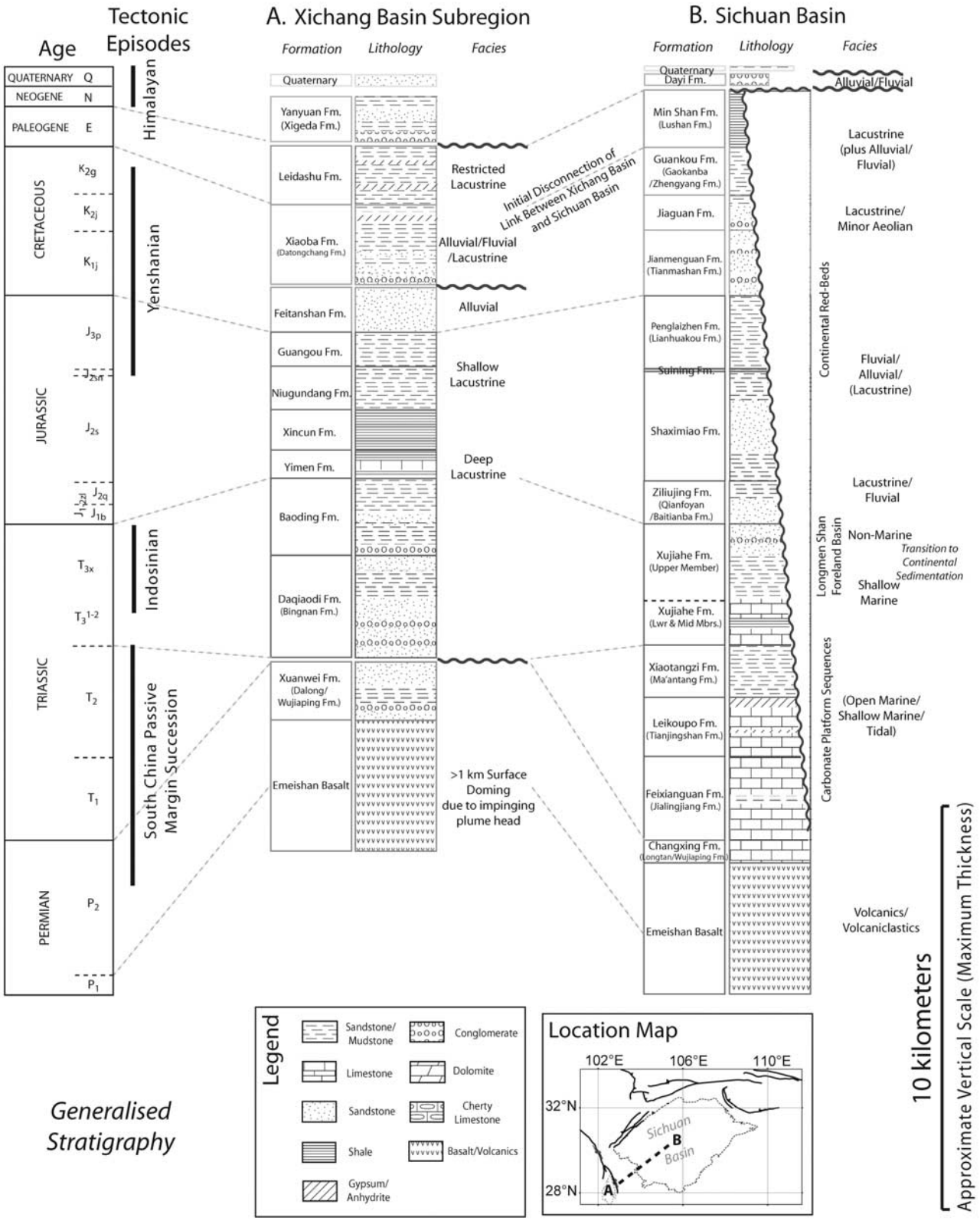

Figure 4. Generalized stratigraphy for the Sichuan Basin, correlated with the Xichang Basin, compiled from *Ma et al.* [2002], *Co-Operative Geological Group of Japan and China in the Panxi Region* [1986], and *Zhang et al.* [1990]. Locations are shown on the inset thumbnail map.

Ratschbacher et al., 2003; *Gilder and Courtillot*, 1997] and resulting in up to 70 degrees of clockwise rotation of the SCB relative to the NCB [*Zhao and Coe*, 1987]. Final closure of the Qinling Suture probably took place during the Middle to Late Jurassic [*Huang and Opdyke*, 1991; *Gilder and Courtillot*, 1997], but continued postcollision convergence developed the East Qinling thrust system [*Mattauer et al.*, 1985; *Wang et al.*, 2003] (Figure 1).

[12] In the western Qinling orogenic belt, exhumation was initiated in the Middle Triassic and continued into the Early Cretaceous, resulting in profound northeast-southwest directed shortening within the Daba Shan [*Wang et al.*, 2003]. Indentors within the SCB located in the Shennongjia and Hannan areas resulted in more intensive deformation in these two zones and the formation of Archean-Proterozoic cored domes with a typical E-W trend [*Cai and Liu*, 1996; *Wang et al.*, 2003]. Through the Cretaceous and early Tertiary, the Qinling Shan almost certainly underwent continuous slow cooling and denudation, as supported by recent apatite fission-track analyses and modeling [*Enkelmann et al.*, 2006].

2.1.3. Southern Margin: Xicang-Yunnan Fold and Thrust Belt

[13] To the south of the Sichuan Basin lies a northwest-southeast trending fold and thrust belt, which became a region of significant Late Cenozoic transcurrent faulting along the sinistral Xianshuihe-Xiaojiang and Red River/Dali Fault systems as a result of the India-Asia collision [*Wang et al.*, 1998].

[14] The Sichuan Basin was probably connected to the Central Yunnan Basin via the Xichang Basin (Figure 1) during the Triassic and Jurassic [*Yang et al.*, 1986; *Co-Operative Geological Group of Japan and China in the Panxi Region*, 1986; *Zhang et al.*, 1990; *Huang and Opdyke*, 1991]. Evidence for this notion comes from the fact that the Jurassic of the Xichang Basin area is dominated by fluvial and lacustrine facies which are lateral equivalents of those in the Sichuan Basin, suggesting that both basins (Figures 1 and 3c) were therefore linked at this time [*Zhang et al.*, 1990]. By the end of the Cretaceous, the depositional environment within the Xichang Basin became fully restricted lacustrine, with deposition of evaporitic gypsum, indicating that a connection to the Sichuan Basin no longer existed [*Zhang et al.*, 1990] (Figures 3d and 4). Closure most probably occurred due to compression of the region, starting at least as early as the Late Jurassic to Middle-Late Cretaceous Yanshan tectonic movement, which resulted in Upper Cretaceous rocks of the Xiaoba Formation being deposited unconformably on top of Middle-Upper Jurassic and Lower Cretaceous strata [*Zhang et al.*, 1990]. It seems likely therefore that higher topography was being developed in this area at least as early as the Middle to Late Cretaceous. Low-temperature thermochronological studies indicate that rapid cooling in the Xianshuihe-Xiaojian region was initiated at approximately 13 Ma [*Clark et al.*, 2005].

2.1.4. Eastern Margin: Hunan-Guangxi Fold Belt

[15] The eastern margin of the Sichuan Basin is formed by a northeast-trending fold and thrust belt with a number of associated open to closed, upright, cylindrical folds that have propagated into the easternmost basin [*Wang et al.*, 1989; *Hsü et al.*, 1990]. Determining the precise timing of the folds in this region is difficult, due to the lack of young sediments, although it is generally assumed that folding and thrusting took place throughout the Mesozoic until at least the Middle Cretaceous (Qianjiang deformation) [*Wang et al.*, 1989] or even Late Cretaceous [*Yan et al.*, 2003]. A number of authors have proposed the existence of an earlier Late Triassic foreland basin on this margin of the Sichuan Basin [*Hsü*, 1989; *Kimura et al.*, 1990; *Wan and Zhu*, 1991; *Korsch et al.*, 1997], although this remains poorly substantiated.

2.2. Stratigraphy

[16] The Sichuan Basin was an area of marine sedimentary deposition almost throughout the Palaeozoic. The primarily carbonate platform conditions of the Permian of the Yangtze Block continued into the Early and Middle Triassic, with a platform-dominated open marine succession in eastern Sichuan, and shallow marine to tidal depositional environments near the western, northern, and southern boundaries of the basin. The Basin became the site of nonmarine sediment accumulation toward the end of the Triassic (Figure 4) [*Burchfiel et al.*, 1995; *Regional Geology of Sichuan Province*, 1991; *Liu et al.*, 1982; *Petroleum Geology of China*, 1987]. A transition from shallow-marine to nonmarine conditions occurred during deposition of the Xujiahe Formation. Sandstone, shale, interbedded coal, and conglomerate (most common in the northern Sichuan Basin) were deposited within the foreland basin with a maximum thickness of over 3000 m adjacent to the Longmen Shan [*Li et al.*, 2003].

[17] Throughout the Jurassic and Cretaceous, large thicknesses of continental red beds accumulated within the basin (Figure 4). During the Jurassic, deformation continued to the north and west of the Sichuan Basin, documented by both the stratigraphic architecture within the basin (Figure 3) and by the presence of conglomeratic alluvial fan deposits along these margins, most notably during the Middle Jurassic. Jurassic strata crop out over much of the Sichuan Basin (Figure 1) and are also significant within the fold and thrust belts to the east and south. These strata are dominated by continental red beds deposited in alluvial, fluvial, and lacustrine environments, with a total residual Jurassic sedimentary thickness of 1 to 3 km.

[18] Cretaceous rocks are only exposed near the western, southern, and northern boundaries of the Sichuan Basin (Figures 1 and 3d). Alluvial fan deposits are present along the westernmost margin of the basin, with discernable fan geometries, and clasts derived mainly from Palaeozoic carbonates exposed within the eastern Longmen Shan. More distal deposits, such as those around Chengdu, are typically lacustrine with minor interbedded evaporitic deposits. Cretaceous rocks towards the south of the basin are more typically red aeolian sandstones within the Jiaguan Formation (Figure 4), overlain by evaporate-bearing mudstones and siltstones of the Guankou Formation [*Liu and Zeng*, 1988]. In the southeastern corner of the basin (Chongqing Province), fluvial sandstones are typical, often with interbedded mudstones.

[19] Strata typically mapped as Eocene on Chinese geological maps are exposed only in the southwesternmost corner of the Sichuan Basin. These strata are poorly dated, due to their continental red bed facies nature. Lithologies are mainly fine-grained red siltstones and mudstones with

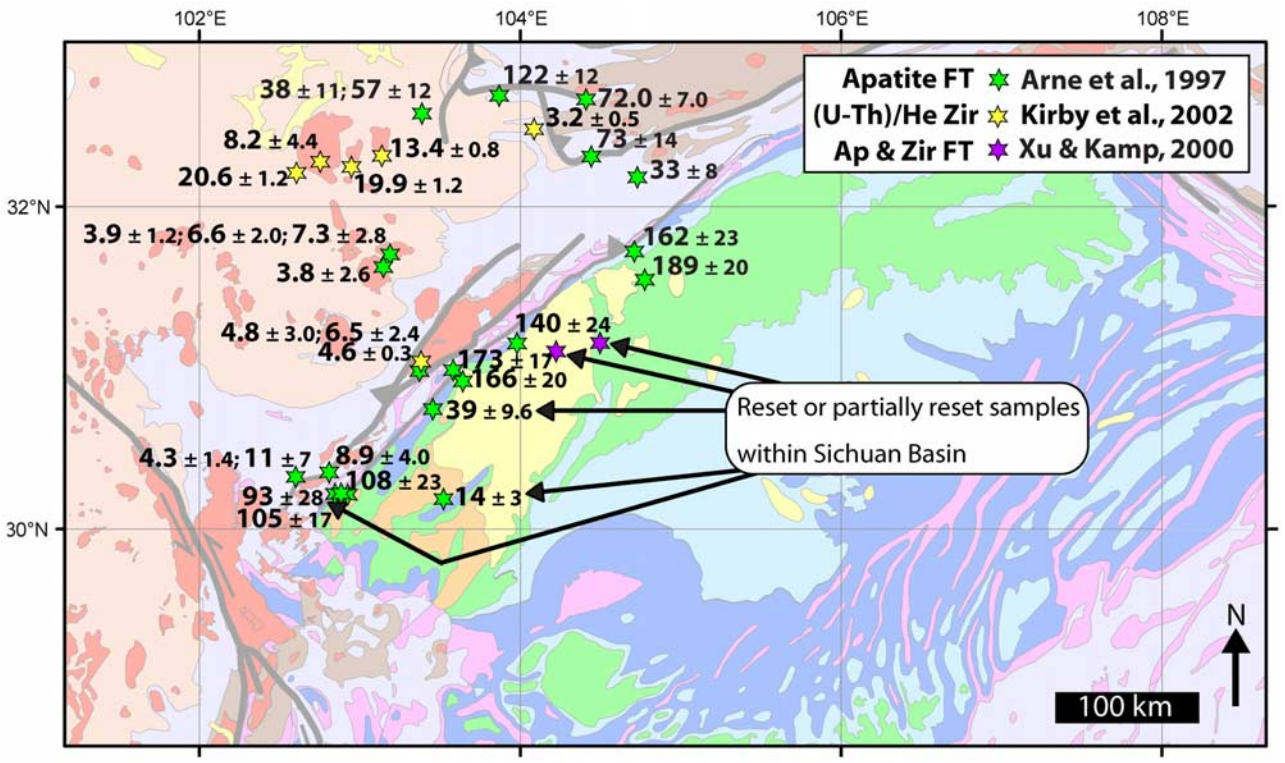

Figure 5. Previously published thermochronological data for the Longmen Shan region. All ages are central ages and are quoted in Ma with 2-sigma errors. Underlying geology from Figure 1 is shown for reference.

thicknesses typically up to a few hundred meters. To the west of Ya'an city, however, there is a thick succession of fluvial and alluvial conglomerate, spectacularly exposed in a gorge to the northwest of Ya'an (295128 E, 3340686 N, UTM zone 48N) which may be up to 1 km in total thickness. Although they only crop out in fairly limited areas, their thickness and lateral facies variations imply that these strata may have been deposited over a much wider region [*Burchfiel et al.*, 1995].

[20] Upper Cenozoic strata are present only within the Chengdu subbasin, confined on their eastern side by the Longquan Shan anticline (Figure 1). Although sequences traditionally mapped as Neogene are thin, they are probably more widespread than previously recognized, since in the past only the well-cemented Dayi and Ya'an conglomerates were mapped as Neogene. The total combined stratigraphic thickness for the Neogene/Quaternary is locally as much as 500 m.

[21] Away from the limited Cenozoic exposures along its western margin, the Sichuan Basin is floored largely by Mesozoic rocks and is currently the site of active erosion over the majority of its surface. Thus a major change from net sediment deposition to net erosion has occurred during the Cenozoic, yet there is little information on the timing and nature of this event. It is additionally important to note that the Upper Cenozoic strata within the western Sichuan Basin lie unconformably over Eocene, Cretaceous, Jurassic, and in some cases Triassic strata. This major unconformity can be correlated laterally with the present day basin surface, at which strata from Eocene to Late Paleozoic ages are exposed. A significant proportion of the Mesozoic and Cenozoic stratigraphic section over the entire extent of the Sichuan Basin has therefore been eroded (Figures 1 and 3).

3. Previous Low-Temperature Thermochronology

[22] A number of previous studies have focused on the thermochronology of the Longmen Shan and the Xianshuihe Fault Zone, with the aim of establishing the timing and rates of denudation associated with growth of the Tibetan Plateau in this region. Only limited studies have so far been conducted on the detrital sediments of the adjacent Sichuan Basin. Apatite fission track studies (AFT), supplemented by $^{40}Ar/^{39}Ar$ (muscovite and biotite) and (U-Th)/He (apatite and zircon) thermochronology (Figure 5), suggest slow regional cooling of the Longmen Shan occurred since the Jurassic, followed by rapid cooling after the Late Miocene with denudation magnitudes of between 8 and 10 km and rates of 1–2 mm/a [*Arne et al.*, 1997; *Kirby et al.*, 2002]. This regional denudational event can be detected at least as far south as the Xianshuihe Fault Zone [*Xu and Kamp*, 2000; *Clark et al.*, 2005], where exhumed zircon fission track partial annealing zones and apatite fission track thermal models indicate that more rapid cooling took place after 11 Ma [*Kirby et al.*, 2002]. This middle to late Miocene increase in cooling has been attributed to increased erosion associated with development of high topography along the plateau margin at this time [*Kirby et al.*, 2002], and even though this denudation may have

Table 1. Apatite Fission Track Data[a]

Sample Number	Irradiation code	Stratigraphic Age	Section Name	Location (UTM Zone 48N, WGS84)	Altitude, m	Number of Grains Counted	RhoD Standard Track Density × 10^5 cm^{-2} (Nd-Counted)	ρs × 10^5 cm^{-2} (Counted)	ρi × 10^5 cm^{-2} (Counted)	Corrected Mean Track Length, μm, Standard Deviation (No. Measured)	P(χ^2), % Variation	Central Age ± 2σ, Ma
0735-2	Eth310-10	Jurassic	Longquan North	449439; 3407242	431	19	9.957 (5824)	6.614 (293)	27.25 (1207)	-	20 (35)	40.3 ± 6.0
0835-1	Eth307-2	Jurassic	Longquan South	413162; 3340028	569	20	11.59 (5074)	5.195 (346)	33.83 (2253)	-	49 (<1)	32.3 ± 6.0
0935-5	Eth310-2	Middle-Upper Jurassic	Guankou	385494; 3438535	670	22	12.61 (5824)	12.89 (678)	18.52 (974)	-	24 (31)	145.5 ± 19.4
1024-3	Eth279-2	Cretaceous?	Longquan North	446702; 3411864	460	20	13.09 (5705)	26.21 (616)	34.51 (811)	-	26 (13)	165.4 ± 24.8
1024-4	Eth279-4	Jurassic	Longquan North	448359; 3407297	461	19	12.48 (5705)	11.48 (287)	28.48 (712)	-	32 (2)	78.7 ± 16.6
1024-5	Eth279-6	Cret/Jurassic?	Longquan North	453737; 3399654	421	20	11.87 (5705)	21.66 (522)	25.02 (603)	-	20 (41)	168 ± 26.0
1024-6	Eth279-8	Cretaceous?	Longquan North	463521; 3395926	450	40	11.26 (5705)	18.82 (1547)	22.34 (1836)	-	98 (<1)	155.5 ± 20.6
1035-1	Eth309-13	Mid-Upper Triassic	Guankou	385557; 3441770	765	20	8.451 (4211)	9.455 (520)	14.55 (800)	-	50 (<1)	94.3 ± 18.2
1324-9	Eth280-4	Jurassic	Xiongpo	367920; 3345295	731	38	12.22 (5931)	5.515 (391)	30.30 (2148)	13.20 ± 1.79 (n = 60)	35 (57)	37.2 ± 4.8
1424-1	Eth280-6	Cret-Eocene Luding Fmn	Ya'an	293563; 3321388	618	23	11.52 (5931)	11.65 (458)	31.60 (1242)	-	40 (1)	72.6 ± 12.2
1424-2	Eth280-10	Middle to Upper Cretaceous	Ya'an	297061; 3323476	612	16	10.12 (5931)	1.884 (117)	19.36 (1202)	-	43 (< 1)	17.9 ± 5.8
1435-1	Eth309-5	Triassic	Emei Shan Anticline	346114; 3278106	687	17	10.75 (4211)	2.96 (209)	31.69 (2237)	-	19 (28)	16.9 ± 3.0
1624-8	Eth280-11	Cretaceous Guankou Formation	Ya'an	282710; 3328748	761	17	9.766 (5931)	6.383 (120)	18.57 (349)	-	13 (71)	55.9 ± 12.2
1735-3	Eth306-3	Lower Jurassic	Weiyuan Anticline	458490; 3272623	377	20	10.32 (4277)	6.706 (454)	36.44 (2467)	-	21 (32)	30.8 ± 4.4
1835-3	Eth307-9	Jurassic	NW of Chongqing	599908; 3310033	329	20	9.910 (5074)	7.587 (434)	18.58 (1063)	-	44 (<1)	62.1 ± 11.6
1835-4	Eth321-8	Jurassic	Central Sichuan	547441; 3328499	329	20	12.12 (4846)	11.879 (354)	19.899 (593)	-	18 (53)	119.9 ± 17.6
1835-5	Eth321-3	Jurassic	Central Sichuan	504008; 3345436	467	16	13.40 (4846)	11.224 (321)	26.993 (772)	-	31 (< 1)	98.2 ± 20.2
2124-1	Eth278-3	Cret/Eocene?	Baitahu, Dayi	364954; 3393586	619	25	12.60 (5705)	13.70 (618)	30.78 (1388)	-	18 (81)	93.2 ± 10.6
2495-1	Eth320-14	Upper Triassic	Eastern Sichuan	218723; 3424223 (zone 49N)	440	20	9.760 (6757)	6.868 (704)	19.66 (2015)	13.47 ± 1.60 (n = 86)	50 (< 1)	54.1 ± 8.8
2495-2	Eth320-10	Lower Jurassic	Eastern Sichuan	219513; 3423039 (zone 49N)	275	20	10.76 (6757)	10.26 (626)	27.79 (1695)	-	28 (8)	66.5 ± 8.2
2495-3	Eth320-7	Middle Jurassic	Eastern Sichuan	220060; 3422079 (zone 49N)	240	20	11.51 (6757)	7.906 (521)	23.07 (1520)	13.53 ± 1.51 (n = 100)	46 (<1)	72.1 ± 13.2

Table 1. (continued)

Sample Number	Irradiation code	Stratigraphic Age	Section Name	Location (UTM Zone 48N, WGS84)	Altitude, m	Number of Grains Counted	RhoD Standard Track Density × 10^5 cm^{-2} (Nd-Counted)	$\rho s \times 10^5$ cm^{-2} (Counted)	$\rho i \times 10^5$ cm^{-2} (Counted)	Corrected Mean Track Length, μm, Standard Deviation (No. Measured)	P(χ^2), % Variation	Central Age ± 2σ, Ma
2595-1	Eth320-3	Lower Jurassic	Eastern Sichuan	677148; 3347814	290	20	12.51 (6757)	11.32 (515)	30.37 1382	-	50 (< 1)	80.9 ± 14.6
2595-2	Eth320-6	Upper Triassic	Eastern Sichuan	676114; 3348416	360	20	11.762 (6757)	12.675 (725)	29.18 (1669)	-	38 (<1)	84.9 ± 12
#300303-6	Eth312-11	Neogene	Baitashan	365043; 3393901	621	30	11.34 (4809)	7.916 (945)	25.257 (3015)	-	0 (22)	61.4 ± 6.8
X1	Eth280-3	Cretaceous	Xiongpo	366337; 3336604	496	20	12.56 (5931)	14.03 (561)	37.00 (1480)	-	32 (3)	83.5 ± 12.0
X2	Eth310-7	Lower Cretaceous	Xiongpo	364996; 3337503	500	20	10.95 (5824)	7.824 (568)	12.74 (925)	-	44 (< 1)	106.9 ± 19.2
X3	Eth310-9	Upper Jurassic	Xiongpo	364310; 3338216	480	20	10.29 (5824)	10.41 (305)	19.49 (571)	-	15 (75)	91.6 ± 14.2
X4	Eth306-8	Upper Jurassic	Xiongpo	363542; 3338535	505	20	9.614 (4277)	10.14 (298)	27.35 (804)	-	71 (<1)	61.9 ± 16.6
X5	Eth309-4	Middle/ Lower Jurassic	Xiongpo	362077; 3340288	692	16	11.15 (4211)	6.250 (185)	29.63 (877)	-	22 (11)	39.8 ± 7.6
X6	Eth309-10	Lower Jurassic	Xiongpo	361101; 3340889	809	20	9.352 (4211)	6.832 (468)	31.14 (2133)	14.09 ± 1.83 (n = 60)	42 (<1)	32.9 ± 6.0
X7	Eth310-12	Upper Triassic	Xiongpo	360337; 3341209	622	22	9.295 (5824)	6.193 (327)	34.74 (1834)	14.25 ± 1.49 (n = 75)	25 (26)	27.5 ± 3.8
*JP1FT6	MU149-6	Upper Jurassic	Borehole	689800; 3486900	−718	40	9.74 (3769)	4.534 (508)	10.41 (1167)	*10.75 ± 0.45 (n = 52)	0 (38)	77.8 ± 14.6
*JP1FT5	MU149-5	Jurassic	Borehole	689800; 3486900	−1644	40	9.58 (3769)	3.72 (463)	15.05 (1873)	*12.02 ± 0.37 (n = 50)	0 (32)	47.5 ± 8.0
*JP1FT4	MU149-4	Jurassic	Borehole	689800; 3486900	−2647	40	9.41 (3769)	3.166 (229)	21.14 (1529)	*10.53 ± 0.74 (n = 17)	80 (0)	25.5 ± 3.8
*JP1FT32	MU149-3	Lower Jurassic	Borehole	689800; 3486900	−3273	14	9.24 (3769)	2.55 (189)	15.18 (1109)	*12.62 ± 0.92 (n = 5)	0 (47)	27.6 ± 8.8

[a]The ρs and ρi represent sample spontaneous and induced track densities, respectively; P(χ^2) is the probability of χ^2 for v degrees of freedom where v equals number of crystals minus 1. All ages are central ages [*Galbraith and Laslett*, 1993]. Here $\lambda_D = 1.55125 \times 10^{-10}$. A geometry factor of 0.5 was used. Lengths were corrected (C-axis projected) using the method of *Ketcham* [2003]. Zeta = 334.6 ± 9 for CN5/apatite (N. Richardson). Irradiations were performed at the ANSTO facility, Lucas Heights, Australia. An asterisk denotes samples analyzed by A. Fowler, where Zeta = 362.3 ± 8 for CN5/apatite and mean track lengths are reported as C-axis uncorrected values. A number symbol denotes sample analyzed by D. Seward, where Zeta = 350 ± 5 for CN5/apatite.

Table 2. (U-Th)/He Data From the Southern Longquan Anticline

Sample	Age, Ma	Error, Ma, 2 sigma	U ppm	Th ppm	He nmol/g	Length, μm	Width, μm
0835-1.1	154.2	8.6	1.35	7.26	1.83	187	189
0835-1.2	15.7	0.5	4.45	16.06	0.51	207	135
0835-1.3	11.5	0.5	1.37	11.97	0.22	163	148
0835-1.4	15.8	0.8	4.62	19.5	0.61	150	108

produced a large quantity of sediment, correlative deposits within the adjacent Sichuan Basin actually have a minor volume [*Kirby et al.*, 2002]. Thus an important puzzle is to determine the amount and timing of sediment erosion or bypass through the basin during the Cenozoic using both onshore (this study) and offshore data sets.

[23] The sparse low-temperature thermochronological data that are available for the Sichuan Basin indicate that at least some postdepositional heating of the Mesozoic basin sediments has occurred. *Arne et al.* [1997] described a number of samples within Triassic to ?Cretaceous sediments along the basin margin that have apatite fission track ages that are less than the sample depositional ages. They attributed this to localized heating, while acknowledging that such an interpretation is problematic given the low density of the sample locations. *Xu* [1997] also conducted a zircon and apatite fission track analysis of boreholes within the western Sichuan Basin and concluded that between 2 and 3 km of denudation took place during the Neogene. More recently, *Enkelmann et al.* [2004] noted two detrital samples in the northwestern Sichuan Basin that yielded AFT ages less than their Jurassic and Triassic stratigraphic ages.

4. Thermochronology

4.1. Fission Track

[24] Fission track dating relies upon atomic-scale damage to the crystal lattice as a result of ^{238}U spontaneous fission decay within the host mineral, in this case apatite. For fission track systems, there are no discrete ''closure'' temperatures as in other radiogenic systems. A transition temperature zone where tracks are essentially unstable is recognized; this is termed the partial annealing zone (PAZ) and is defined by upper and lower temperature limits that are dependent on cooling rates. The PAZ for apatite lies between approximately 60° and 120°C [*Laslett et al.*, 1987; *Corrigan*, 1993] with an effective closure temperature of 110 ± 10°C. Hence apatite fission track analysis is particularly useful for evaluating low-temperature thermal histories, that is, those affecting the upper 3–4 km of the crust.

[25] Throughout this study, we deal with the thermal history of detrital apatite grains. The fission track method allows us to derive information which can reflect not only the thermal history of the sediment in question but also that of the hinterland from which the grains have been initially derived. A sample that is unreset since deposition will retain the thermal history of the source region and will yield a fission track age that is greater than its stratigraphic age [e.g., *Ruiz et al.*, 2004]. A sample with partially reset apatites has been modified by a thermal overprint, thus changing the original detrital age and confined track length distribution. Such partially reset samples may thus contain a proportion of individual grains that are less than the stratigraphic age, while those that retain the detrital signature yield ages that are exclusively older than the depositional age of the host sediment. The probability of a population of single grain ages belonging to a single population is assessed by the chi-square statistic [*Galbraith*, 1981]. In general, a chi-square probability of less than 5% is a good indicator of partially reset or detrital ages. Partially reset samples will yield a range of single grain ages that may be younger than, equal to, or older than the sample's stratigraphic age. Detrital samples yield ages exclusively older than the depositional age of the host sediment (although sometimes other information may be needed to confirm that these have not suffered some small degree of heating yet still maintain an age that is older than the stratigraphic age.) Samples that are fully reset have been heated to such a degree that no hinterland information is retained, the original fission tracks within the sample have been totally annealed, and the sample (and all individual grains within it) will yield ages that are less than the stratigraphic age. Determining the depth at which total annealing occurs may require additional information such as a suite of downsection samples to establish variations in the degree of downhole annealing.

4.1.1. Analytical Procedure

[26] Fission track sample preparation followed routine techniques for separation of apatites [*Seward*, 1989]. Etching of all apatites except those from borehole JP1 was done at ETH Zurich with 7% HNO_3 at 21°C for 50 s. This etch time yields similar track length parameters to the etch using 20 s in 5N HNO_3 [*Seward et al.*, 2000] used in the annealing studies of *Laslett et al.* [1987] and for the etching of apatites from borehole JP1 at the University of Melbourne. Muscovite detectors were etched in 40% HF for 45 min at room temperature. All irradiations were carried out at the ANSTO facility, Lucas Heights, Australia. Microscopic analysis was undertaken using a Zeiss Axioplan2 optical microscope with a computer-driven stage and FTstage 4 software from *Dumitru* [1995]. All ages were determined using the zeta approach [*Hurford and Green*, 1983] with a zeta value of 334 ± 9 (Richardson) and 362 ± 8 (Fowler) for CN5 dosimeters. They are reported throughout this paper as central ages [*Galbraith and Laslett*, 1993] with a 2σ error (Tables 1 and 2). Where possible, at least 20 crystals of each sample were counted for age determination. The magnification used was 1250X for determining both apatite track densities and horizontal confined track lengths.

4.1.2. Modeling

[27] Temperature-time paths were derived for each modeled sample through inverse Monte Carlo modeling using the HeFTy software of *Ketcham* [2005]. Since all of the samples used in this study were clastic sediments (sandstones and silty sandstones), consideration of the known sedimentary basin history allowed us to place some constraints on the manner in which they were modeled. As an initial constraint, we allowed the sample to cool from any temperature above, within, or below the PAZ to simulate uncertainty in the initial thermal history inherited from the sedimentary source. The sample was then constrained to be at or near the surface at the approximate time of sedimentary deposition and was then unconstrained between deposition and the present day. The track modeling philosophy was to

limit the modeled path as little as possible beyond these first order assumptions, so large constraint boxes were chosen to allow the model as much freedom as possible. Between constraints, paths are monotonic consistent with episodic randomization and halving of the path four times to allow for sufficient variability in the exhumation path.

[28] The kinetics of fission track annealing have been found in many instances to be a function of chemical composition [e.g., *Gleadow and Duddy*, 1981; *O'Sullivan and Parrish*, 1995]. *Burtner et al.* [1994] have shown that this amounts to a variation in total annealing temperature by as much as ± 20°C in extreme cases. The mean track pit diameter of the apatites in this study (1.8–5.0 μm within some extreme samples) suggests that the apatites possess a range of chemical compositional variability. Hence we used the annealing model of *Ketcham et al.* [1999], which takes into account the chemical variability by using the diameter of etched tracks at the surface of the apatite (Dpar) as a proxy for the annealing kinetics of the grains. The Dpar kinetic parameter was also used to calculate initial confined track lengths. Length corrections were made to account for variability in track length that reflects anisotropy of annealing and etching dependent on angle to the crystallographic C-axis using the method of *Ketcham* [2003]. The Kolmogorov-Smirnov statistical test was used to assess the goodness of fit between modeled and measured track length distributions, with merit values of 0.5 and 0.05 for good and acceptable fits, respectively.

4.2. (U-Th)/He Dating

[29] The (U-Th)/He dating method is based on the accumulation of radiogenic helium as a result of α-decay from uranium and thorium, and to a smaller extent from samarium, within mineral grains. As with fission tracks, He is variably retained in the crystal within a range of temperatures, termed the partial retention zone, that are partly dependent on cooling rate. The effective He closure temperature in apatite has previously been estimated to be 68 ± 5°C [*Wolf et al.* 1996; *Farley*, 2000]. Measured (U-Th)/He ages are a reflection of the competing effects of in situ radiogenic He production and diffusive loss of He. This technique is becoming increasingly important in studies of exhumation and erosion since it documents cooling within the uppermost portion of the crust.

4.2.1. Analytical Procedure

[30] For reliable (U-Th)/He analysis, sufficiently large (>100 μm across), inclusion-free apatite crystals could only be selected from one detrital sample (0835-1), for which multiple grains were analyzed (Table 2). Crystals were handpicked using a binocular microscope under polarized light at 200X magnification and the crystal length and width was measured electronically to allow calculation of the α-ejection correction according to *Farley et al.* [1996]. Crystals were wrapped in pure platinum foil to allow homogeneous heating with an infrared Nd-YAG laser (1064 nm wavelength) to temperatures in the range of ~1100°C for 3 min. Gas released inside the laser chamber was expanded into an ultra-high vacuum with H_2O and CO_2 frozen out using a liquid nitrogen-cooled cold trap, argon trapped on a cold charcoal finger, and subsequent cleaning using Ti/Zr getters. Helium was then measured using a dedicated noble gas sector field mass spectrometer (''Albatross,'' 90°, 21 cm radius). Blank measurements were regularly run between samples to allow corrections to be made. Reheating of apatite grains was performed in order to verify complete degassing. Uranium and thorium contents of the same crystals were subsequently determined by Multiple Collector Inductively Coupled Plasma Mass Spectrometry (MC-ICPMS). The degassed crystals were spiked with a $^{233}U/^{229}Th$ solution and digested at ~100°C using 1.5N HNO_3 with trace HF. U and Th were separated using TRU ion exchange resin (Eichrom), treated using H_2O_2 and dissolved in ~1 ml 0.3N HNO_3-0.1N HF which was aspirated into the plasma source of a Nu Plasma MC-ICPMS. Measured isotopic ratios were corrected iteratively for small contributions of natural isotopes present in the spike tracer, instrumental mass bias, and ion counter gain. Further analytical details are documented by *Wipf* [2006].

5. Results and Interpretation

5.1. Apatite Fission Track Thermochronology

[31] Apatite fission track results are shown on the map in Figure 6 and are reported in Table 1. All samples of Cretaceous stratigraphic age yielded fission track central ages that were older than their depositional age, indicative of no or little resetting. All Jurassic and Triassic stratigraphic samples yielded fission track central ages that were less than their depositional age, indicating partial to full resetting and a first-order tendency toward younger fission track ages at deeper stratigraphic levels. This indicates that there has been basin-wide thermal heating of these sediments, and the fact that older strata are most affected by this fission track resetting indicates that the most likely cause is burial by sedimentation. Fully reset ages are primarily found within eroded anticline cores, since these reveal deeply buried Triassic rocks which are not otherwise exposed at the basin surface (Figure 6). However, it is important to note that the thermal resetting of these samples is unrelated to folding, since fully reset Triassic samples are also found at relatively shallow depths in borehole JP1 (Figure 6) and in other boreholes within undeformed parts of the basin [*Xu*, 1997].

[32] We note that while we present central ages of unreset and partially reset samples, the central age of such samples may not be representative of the entire single-grain age population, as discussed by *Vermeesch* [2004], and the meaning of such an age is somewhat open to question. Nevertheless, most ages presented here are partially to fully reset and the central apatite ages at least provide a first-order indicator of the amount of annealing when considered together with the stratigraphic age.

5.1.1. Xiongpo Anticline

[33] To better illustrate the general pattern of resetting and to extract information on the timing and magnitude of burial and denudation, we focus on the most complete preserved stratigraphic section, exposed in the Xiongpo Anticline in the western Sichuan Basin (Figures 7 and 8). Within this section, the top and base of an exhumed paleopartial annealing zone (paleo-PAZ) have been exposed, allowing us to put constraints on both the amount of missing stratigraphic section, and the timing of the exhumational event. The Xiongpo Anticline (Figure 7) exposes a continuous section from the Upper Triassic Xujiahe Group through to the Upper Cretaceous Guankou Formation (and

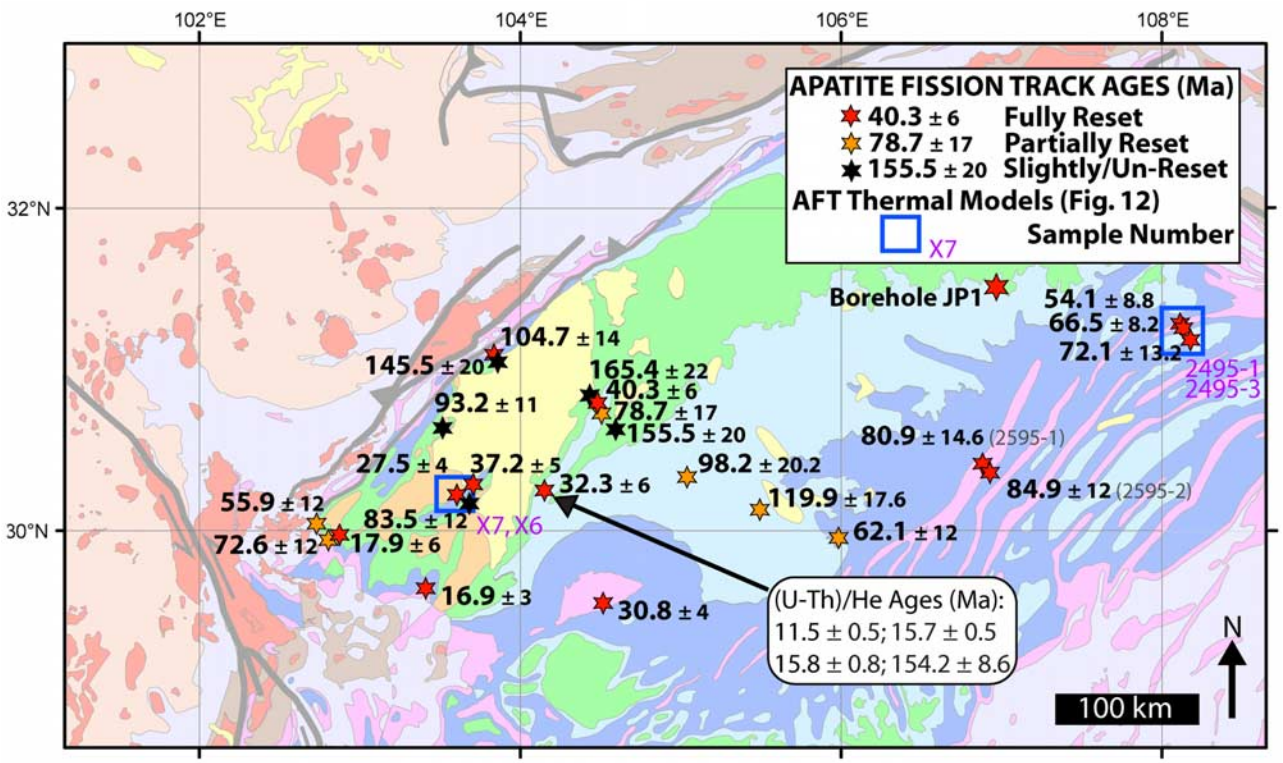

Figure 6. New thermochronological data for the Sichuan Basin region (this study). All AFT ages are central ages and are quoted in Ma with 2-sigma errors. Underlying geology from Figure 1 is shown for reference. Red stars indicate fully reset detrital samples (those where all grains within the sample are less than the stratigraphic age), orange numbers indicate partially reset detrital samples (in which only some of the grains are less than the stratigraphic age), black numbers indicate slightly to unreset detrital samples (in which all the grains analyzed are older than their stratigraphic age). Blue boxes show locations of samples used in thermal modeling (Figure 10).

along-strike nearby the Eocene Min Shan Formation), which is unconformably overlain by the late Neogene (probably Plio-Pleistocene) Dayi Formation. Because of the uncertainty in the stratigraphic ages of the samples, we have assigned arbitrary but generous error margins of ±20 Ma to the stratigraphic ages. In the discussion below this error margin is considered.

[34] The stratigraphically youngest sample within this section (X1, Upper Cretaceous) yields a population of single grain ages that are generally older than the stratigraphic age (depending on the accuracy of this age) (Figures 8 and 9). This sample, as with samples X2-X4 in the uppermost portion of the section, shows a wide spread in single grain ages. Samples progressively further down the stratigraphic section yield an increasing proportion of single grain ages that are younger than their stratigraphic ages (Figures 8 and 9), reflecting an increased degree of resetting with stratigraphic depth. The three stratigraphically oldest samples at the base of the section (samples X5, X6, and X7) have a narrow spread in single grain ages, all of which are significantly younger than the stratigraphic age (Figures 8 and 9). On the basis of these observations, it is possible to make an estimate of the bounding limits of the paleo-PAZ. The top of this zone most likely lies between samples X1 and X2 (approximately 400 to 500 m stratigraphically below the Cretaceous-Neogene unconformity), while the base is somewhere close to samples X5 and X6 (approximately 2500 to 2600 m below the unconformity), where all the detrital ages are clearly very much younger than the stratigraphic ages. In addition, the central ages of the lowermost three samples decrease systematically with depth in accordance with their relative timing of exhumation (as in an age-altitude plot). Samples X5 and X6 lie in close proximity to the base of an exhumed partial annealing zone. We note that the exact location of the top and base of the PAZ is somewhat dependant on uncertainty in the stratigraphic ages of the samples as mentioned above. The continental strata from which the samples are derived have been correlated to sections that have been studied using paleontological [*Liu et al.*, 1982] and paleomagnetic techniques [*Enkin et al.*, 1991a, 1991b; *Huang and Opdyke*, 1991; *Yokoyama et al.*, 2001]. Although we have given the age of the strata a generous error range, we are confident the apatite fission track ages have been correctly classified as either nonreset, partially reset, or fully reset. Importantly, the mean track lengths of horizontal confined fission tracks (after correction for C-axis orientation effects) within the lowermost samples are relatively long, with mean track lengths of 14.09 ± 1.83 μm for sample X6 and 14.25 ± 1.49 μm for sample X7. Such long track lengths are supportive evidence for full annealing of these detrital samples whose central ages thus reflect purely postdepositional cooling

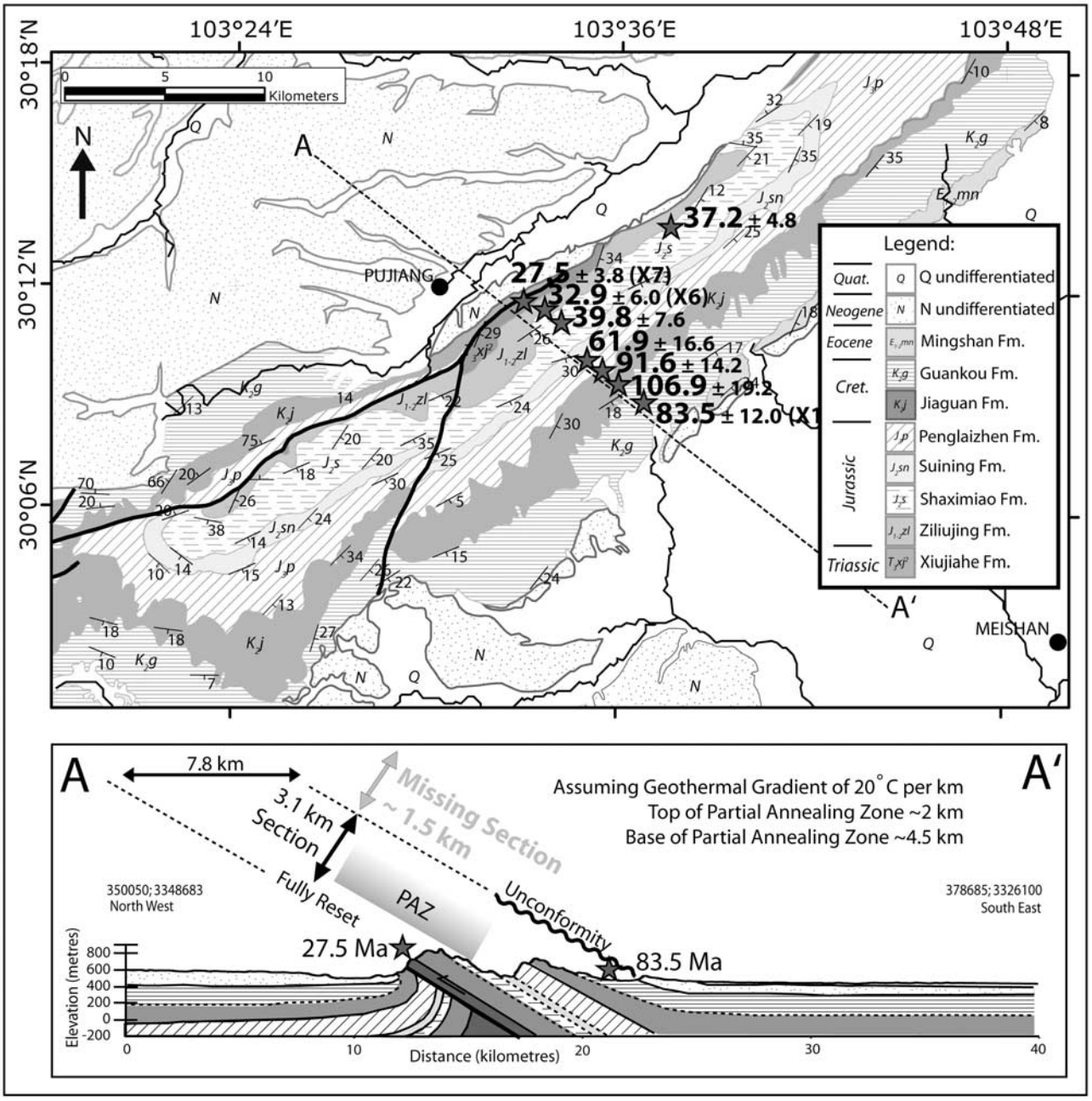

Figure 7. Detailed geological map of the Xiongpo Anticline. Apatite fission track sample locations are marked with stars and their associated apatite fission track central ages are given in Ma, with 2-sigma errors (selected sample numbers in brackets). See Figure 1 for location. Lower half shows structural cross section A-A' across the Xiongpo anticline.

through the AFT closure temperature. Sample X5 (central age 39.8 Ma), which lies closest to the base of the exhumed paleo-PAZ, probably most closely reflects the timing of the onset of rapid postdepositional cooling.

5.1.1.1. Magnitude of Exhumation

[35] The stratigraphic section of the Xiongpo Anticline also allows us to estimate exhumation magnitudes, as the amount of section between the top and base of the PAZ can be used to derive a geothermal gradient based upon the temperature zone spanned by the PAZ. On the basis of the relative depths of samples X1/X2 and X5, the PAZ is approximately 2 km thick, and since the top of the PAZ occurs at $\sim$ 60°C and the base at $\sim$ 110°C (i.e., a difference of 50°C), the calculated geothermal gradient is 25°C km^{-1}. With these assumptions, and given an average surface temperature of 15°C, we would expect temperatures of $\sim$60°C (top of the PAZ) at a depth of approximately 1.8 km below the surface and temperatures of $\sim$110°C (base of the PAZ) to be reached at a depth of approximately 3.8 km. However, the top and base of the paleo-PAZ in the measured section are only $\sim$500 m and $\sim$2500 m below the unconformity, respectively, so there must be stratigraphic

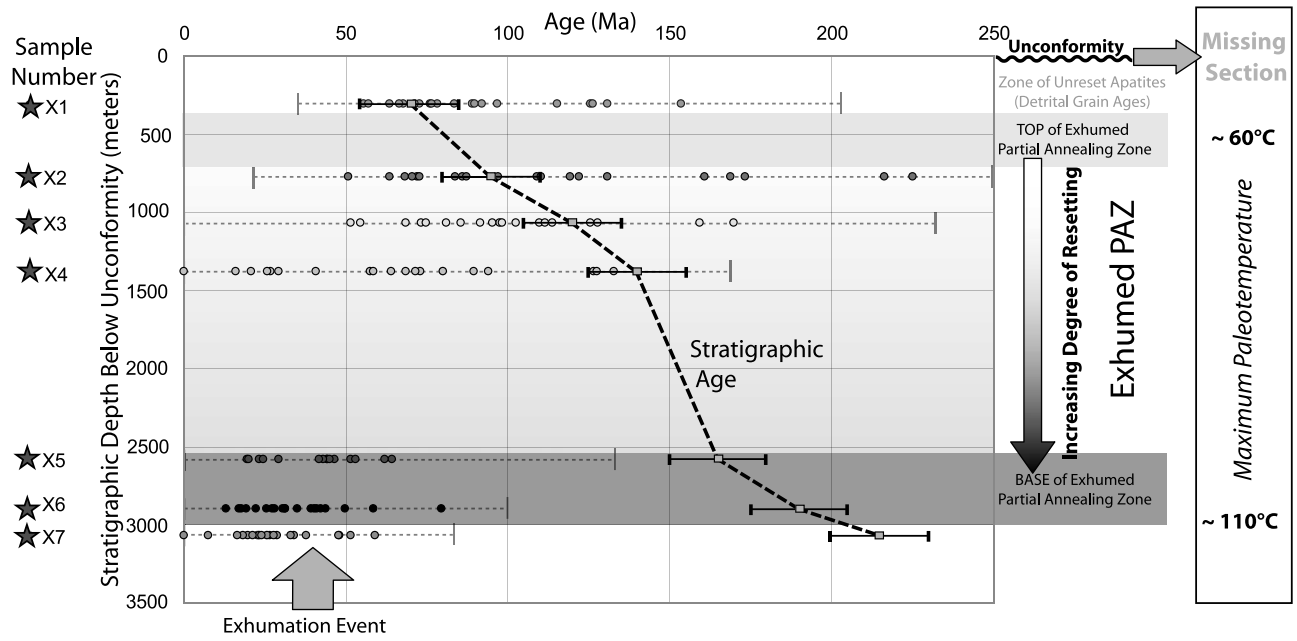

Figure 8. Single-grain apatite fission track ages for samples across the Xiongpo Anticline plotted against stratigraphic depth below the Cretaceous-Neogene unconformity. See Figure 7 for sample locations. Squares show the stratigraphic age of each sample. Errors in the stratigraphic ages are assumed to be ± 20 Ma and are shown by solid black error bars. Single-grain ages decrease downsection, reflecting the increasing degree of fission track resetting with depth. The range of two-sigma errors for the single grain ages are shown by thin dashed lines. The top of the partial annealing zone is most likely located between samples X1 and X2 (where the number of single grain ages younger than the stratigraphic age starts to increase). Samples X5, X6, and X7 are defined as being fully reset (since all single grain ages are less than the stratigraphic age); therefore the base of the exhumed AFT paleopartial annealing zone lies somewhere close to 2500 m stratigraphically below the unconformity. By assuming a time- and depth-invariant geothermal gradient of 25°C per km and a surface temperature of 15°C, and taking 60°C and 110°C as the top and base of the AFT partial annealing zone, we calculate that at least 1.3 km of the stratigraphic column must be missing.

material missing from the upper section (Figures 8 and 9). On this basis, the total missing section is approximately 1.3 km at this location.

[36] Although we have assumed in the above calculation that the geothermal gradient is fixed through time, it is more likely to have varied since the Late Triassic, with a geologically conceivable range of 15 to 35°C km^{-1}. Taking the extremes within this range, the magnitude of the eroded material may be as low as 0.25 km (geothermal gradient of 35°C km^{-1}, base of PAZ at ~2.75 km) but as high as 4.1 km (geothermal gradient of 15°C km^{-1}, base of PAZ at ~6.6 km). Present day borehole temperatures for this area indicate a geothermal gradient of ~20°C km^{-1} in the upper few km of the basin [*Xie and Yu*, 1988] and low heat flow [*Hu et al.*, 2000]. In addition, the geothermal gradient has probably not been greatly above this value since the formation of the Late Triassic Longmen Shan Foreland Basin, when the heat flow was more likely even lower based on comparisons with other foreland basins [*Allen and Allen*, 1990; *Schegg and Leu*, 1998], due to the lack of any subsequent extensional or volcanic activity in this region. Since the geothermal gradient in stable crust is largely a function of erosion rate, and throughout the Mesozoic the basin was depositional, it is likely therefore that the geothermal gradient would be on the low side of normal, (i.e., between 20 and 25°C km^{-1}). Plate interior settings experiencing relatively low erosion rates (~1mm/a) typically have geothermal gradients of less than ~ 25°C km^{-1} (e.g., Colorado Plateau). Total postdepositional denudation of 1.3 km thus represents a conservative but realistic estimate of the amount of material eroded at this location.

5.1.1.2. Timing of Exhumation

[37] The onset of cooling can also be constrained by modeling of horizontal confined tracks that were measured for the samples (Figure 10). Here we present a pair of closely spaced, fully reset samples from the Xiongpo Anticline (samples X6 and X7, central ages 32.9 Ma and 27.5 Ma, respectively), The thermal models for these two samples indicate that following deposition (Figure 10, box D), they are likely to have reached their maximum burial depth during the Early Tertiary, consistent with the knowledge that they are covered by Jurassic to Eocene sediments (Figures 7 and 8). Both models indicate that following burial, the onset of cooling to present-day exposure took place no earlier than 40 Ma and certainly no later than ~25 Ma.

[38] That this cooling event is not the result of focused exhumation above the fold can be demonstrated by consideration of the local stratigraphy. On both the eastern and western limbs of the Xiongpo Anticline, Mesozoic strata are cut by an unconformity (disconformity) capped by the

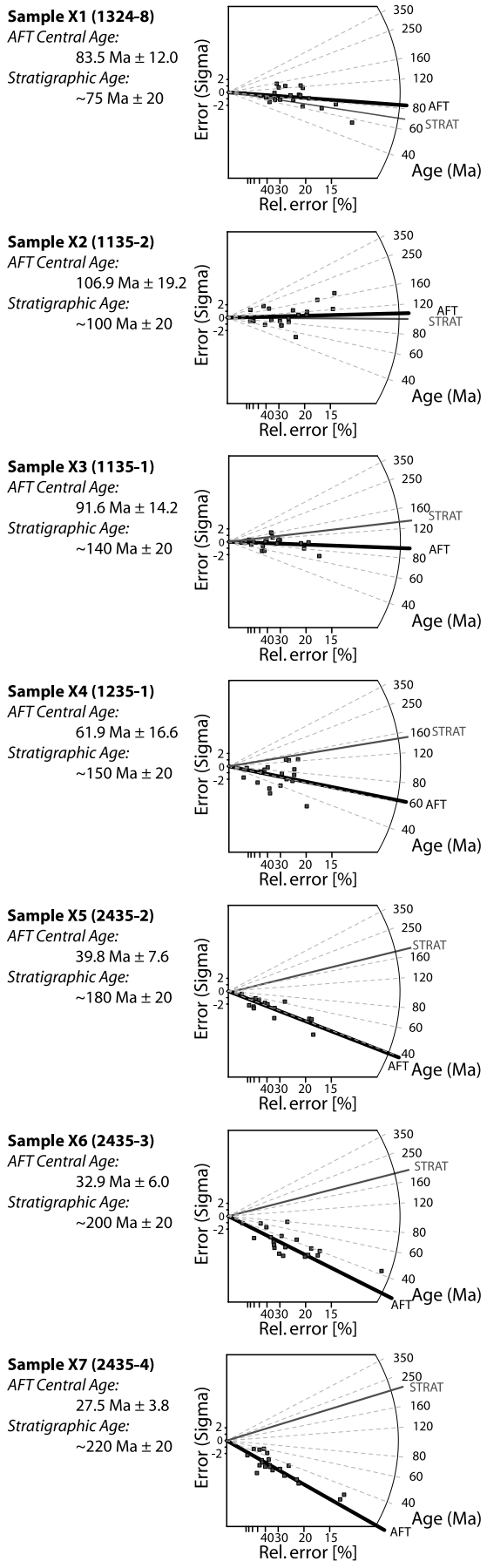

poorly consolidated Neogene Dayi Formation. As pointed out by *Burchfiel et al.* [1995], dating these Neogene strata is crucial to determining the timing of deformation on the Xiongpo Anticline. Apatite fission track ages of individual detrital grains within the Neogene strata allow us to place a maximum age on the depositional age. Detrital ages from sandstone within the Dayi Formation (Figure 11, Location: 364967; 393960; 615 m) indicate that these strata are no older than 12 ± 4 Ma, the age of the youngest grain. Additionally, since these Neogene strata are overturned on the western limb of the fold, the deformation must also be younger than ~12 Ma. The fact that correlative sediments are present on the eastern limb of the anticline, which now acts as a barrier to sediment supply from the Longmen Shan, combined with the observation that the Neogene sediments do not contain clasts of the underlying formations which could have been shed off an emergent structure, indicates that there was no topographic expression of the Xiongpo Anticline at the time of sediment deposition. Erosion and formation of the Cretaceous-Neogene unconformity therefore predates the folding, and must have occurred prior to ~12 Ma. Thus although focused denudation has obviously occurred above the Xiongpo Anticline since ~12 Ma, formation of the Cretaceous-Neogene unconformity at this location occurred in an earlier exhumation event, which most likely initiated during the Middle to Late Eocene.

[39] Samples higher up the stratigraphic section did not yield sufficient grains of the requisite quality and crystallographic orientation to allow meaningful analysis of track length distributions through the entire sample suite. In any event, the track length distributions for these samples would reflect the inherited detrital track distributions, overprinted with the signature of thermal reheating, and thus the derivation of a meaningful thermal history for these samples would be problematic.

5.1.2. Borehole Data

[40] An additional suite of samples was obtained from borehole JP1 located in the central-northern part of the Sichuan Basin (Figure 6), geographically removed from both the anticlines within the basin and the structurally deformed margins. The deepest sample, JP1FT4 has a central age of 25.5 ± 3.8 Ma with a high chi square value of 80 and 0 % variation, suggesting that it has been fully reset and the age approximates the timing of cooling through the closure temperature for that site. On the other hand, sample JP1FT5 has an apparent age of 47.5 ±8 Ma, a chi-square value of zero, and a variation of 32%. One single-grain age in JP1FT5 is older than the estimated stratigraphic age, and the mean track length is 12.0 ± 2.6 μm, suggesting that the sample was not quite fully reset, and lies close to the base of the paleo-PAZ. Thus this downhole transect (Figure 12) reveals the base of a paleo-PAZ at

Figure 9. Radial plots for apatite fission track samples in the Xiongpo area (see Figures 1, 7, and 8 for sample locations). The apatite fission track central age is plotted as a solid line marked "AFT," and the stratigraphic age of each sample is plotted as a solid line marked "STRAT." This diagram clearly reveals the increasing degree of resetting with stratigraphic depth.

present-day depths of between ~1650 m and ~2650 m and temperatures of between ~48 and ~68°C, indicating that these strata have undergone significant cooling since they reached peak paleotemperatures of around 110°C. This cooling is consistent with the removal of ~2 km of sedimentary cover, assuming that the current geothermal gradient of ~18°C km^{-1} is representative of the geological history of these samples. Hence the initiation of cooling was most likely between the apparent ages of samples JP1FT4 and JP1FT5 (i.e., between 25.5 ± 8 Ma and 47.5 ± 8 Ma). Because the borehole lies in an undeformed area of the Sichuan Basin and yet shows broadly similar timing and magnitude of denudation as the Xiongpo Anticline, we further conclude that resetting of Jurassic and Triassic samples is unlikely to be due to localized erosion of folds.

5.1.3. Central and Eastern Basin

[41] We also analyzed an east-west transect of Jurassic detrital surface samples across the center of the basin, away from the effects of any deformation (samples 1835-3, 1835-4, and 1835-5). These samples contain a majority of grains that yield AFT ages less than the stratigraphic age of the host strata, with central ages of 62.1 ± 11.6, 119.9 ± 17.6, and 98.2 ± 20.2 Ma (Figure 6). To be reheated to a degree that would allow such partial resetting, these samples would have been buried to depths in excess of approximately 2 km since their deposition, given assumptions about the geothermal gradient similar to those used for the Xiongpo Anticline and for the JP1 samples. This cannot be due to localized exhumation, since the samples are far removed from any anticlines and are spaced widely across the center of the basin.

[42] Two sample transects from anticlines in the eastern Sichuan Basin yielded five dateable samples (2495-1, 2495-2, 2495-3, 2595-1, and 2595-2, Table 1, Figure 6) in which single grain ages are also less than the samples' depositional age. Although these samples have a relatively wide spread in single grain ages (radial plots; auxiliary material Figure S1[1]), all the single grain ages are much younger than the host stratigraphic age, in accordance with being fully to almost fully reset after deposition. The mean lengths of 2495-3 and 2495-1 are 13.68 and 13.47 μm, respectively, with no track lengths smaller than 9 μm, also supporting the notion of full resetting after deposition. These lengths and the wide spread in the radial plots reflect slow cooling through the PAZ since the Cretaceous, and this is demonstrated in thermal models of two of these samples (samples 2495-1 and 2495-3, central ages 54.1 and 72.1 Ma, respectively; Figure 10). These two inverse thermal models exhibit a slightly different cooling history compared to those in the Xiongpo Anticline, with the onset of relatively slow cooling through the lowermost PAZ during the Middle-Late Cretaceous, followed by an increase in cooling rate sometime after 40 Ma, as indicated by the break in slope of the cooling pathway. This break in slope is necessary to produce a statistically acceptable model fit; constant cooling since about 70 Ma is outside the bounds of what is possible according to the models. This Middle to Late Eocene change in cooling rate is consistent with the changes identified across other parts of the basin. The slower thermal cooling that initiated before this time in the eastern Sichuan Basin may reflect the initiation of compressional tectonics and associated erosion within the Hunan-Guangxi-Eastern Sichuan fold belt, which is consistent with the study of *Yan et al.* [2003].

[43] The Middle to Late Eocene change in cooling rates across broad areas of the central and eastern Sichuan Basin demonstrates that significant denudation extended over a large area and was of a magnitude sufficient enough to bring partially and fully reset rocks at the surface.

5.2. (U-Th)/He Dating

[44] To extend the thermal histories derived above to lower temperatures, four grains from one sample locality were analyzed using the (U-Th)/He method. The samples were all derived from a coarse-grained Jurassic sandstone at the southern end of the Longquan Anticline (Figures 1 and 6). Single-grain ages for the sample are 11.52 ± 0.27, 15.66 ± 0.23, 15.83 ± 0.40, and 154.24 ± 4.32 Ma (Table 2). The first three ages are, as expected, younger than the detrital apatite fission track age for the same sample (32.3 ± 6 Ma), consistent with full resetting of the sample and cooling through both the PAZ and the apatite He partial retention zone during Cenozoic denudation. The latter age is anomalously high and probably does not represent a true cooling age because it is much older than the apatite fission track age. This may be due to a number of factors including zonation or implantation with helium (see *Fitzgerald et al.* [2006] for a full discussion).

6. Discussion

[45] Our results demonstrate that widespread erosion of at least 1.3 km magnitude has taken place across the Sichuan Basin at some point after the late Middle to Late Eocene. Throughout the Mesozoic, the basin accumulated sediment derived from the enclosing mountains. The Sichuan Basin, however, is now hydrologically and sedimentologically open, drained by the Yangtze River and its tributaries, with much of the basin floor characterized by nondeposition or erosion. Thus a major change in the drainage system of the Sichuan Basin must have occurred since the Early Tertiary. Below, we summarize evidence for widespread denudation in the Sichuan Basin, outline potential mechanisms by which this could have occurred and describe the effects of this denudation on areas to the east and west of the basin.

6.1. Evidence for Widespread Denudation

[46] Our low-temperature thermochronological data allow us to constrain the magnitude, areal extent, and time of initiation of Cenozoic erosion. Detrital apatite fission track samples from Jurassic and Triassic strata across the basin repeatedly exhibit AFT grain ages that are less than the depositional age of the host strata. The degree of resetting alone indicates the maximum temperature (and therefore the depth) to which a sample has been subjected. Samples which are partially thermally reset indicate maximum paleotemperatures of >60°C (equivalent to burial of ~2 km and possibly more), and those which are fully reset indicate maximum paleotemperatures of >110°C (equivalent to burial below ~4.5 km depth). Since such thermally reset samples are exposed at the current surface of the basin, the

[1] Auxiliary materials are available in the HTML. doi:10.1029/2006JB004739.

thickness of sedimentary material removed from much of the basin must equal or exceed these values. Stratigraphic sections allow us to further constrain both the timing and magnitude of the cooling event. Apatite fission track ages of reset samples and thermal models from within the basin indicate that exhumation was initiated at some time after about 40 Ma.

[47] Other indications that a large amount of sedimentary material has been removed from the Sichuan Basin come from ongoing petroleum exploration studies. Although higher than expected vitrinite reflectance measurements have been noted by Chinese petroleum geologists for the last few decades, this was previously considered to be a result of much higher than present geothermal gradients [*Wu and Wu*, 1998]. We discount this on the basis that the western and northern margins of the basin have acted as foreland basins since the Late Triassic and must therefore have had commensurately low geothermal gradients from this point in time onward. The Sichuan Basin has not experienced any major extensional or volcanic events for at least the last 250 Ma, and so the geothermal gradient probably remained fairly low, and presumably close to a value of 20 to 25°C km^{-1}, typical for such a continental interior setting. The most feasible option to explain such widespread elevated paleotemperatures must therefore be heating during burial, followed by cooling due to erosion. Backstripping of borehole data [*Korsch et al.*, 1997] suggests that maximum burial probably occurred in Late Cretaceous to Early Tertiary time, shortly before the initiation of the basin-wide erosional event constrained by our data to <40 Ma.

[48] Finally, geological evidence supports the notion of widespread, post-Cretaceous to post-Eocene erosion. Through the Phanerozoic, the Sichuan Basin developed as a sedimentary depocenter enclosed on all sides by orogens. Areas within the basin have remained undeformed except at relatively shallow crustal levels (for example in the eastern Sichuan fold and thrust belt). In contrast, major compressive and transpressive deformation has occurred on all four boundaries of the Sichuan Basin since the Triassic. Deposits in the sedimentary basin have been continental since the latest Triassic, and both Jurassic and Cretaceous sediments are of alluvial fan, fluvial, and lacustrine facies types, with a significant proportion of the material derived from the surrounding topographic highs and no evidence of sediment bypass through the basin at this time.

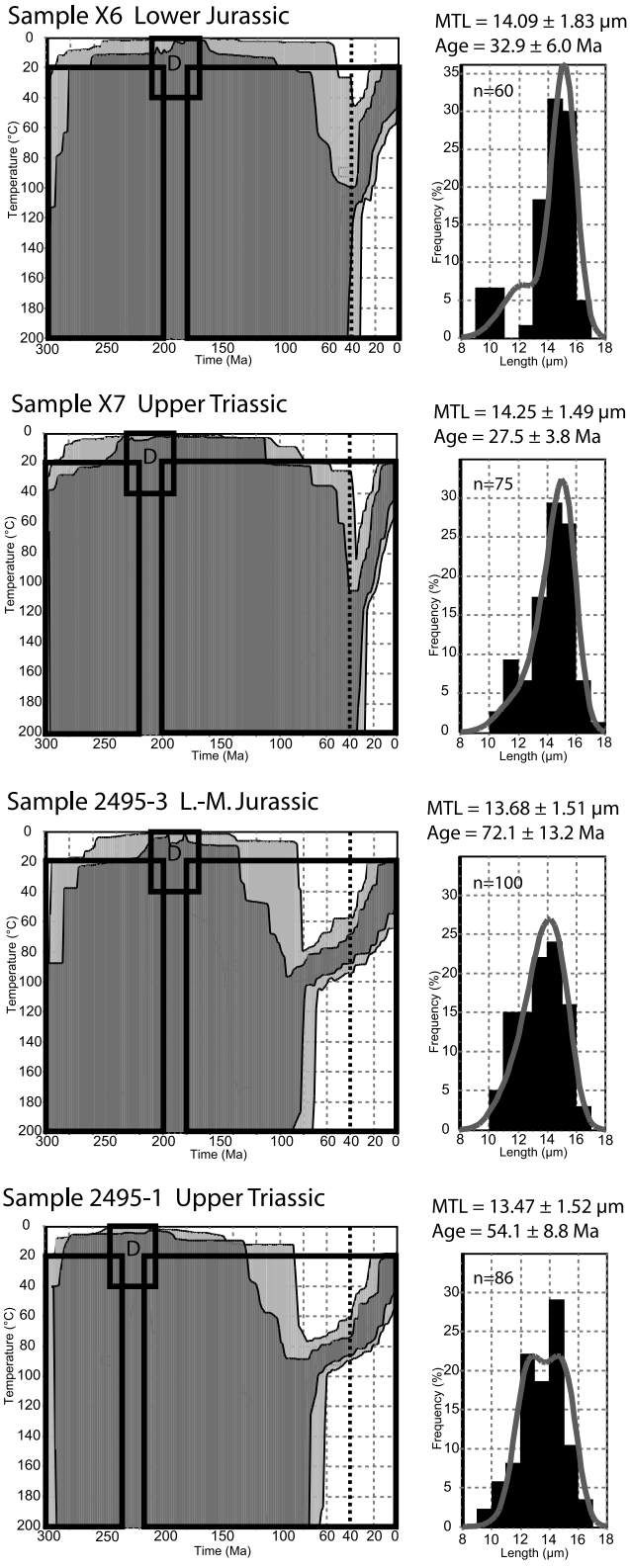

Figure 10. Monte Carlo inverse temperature-time models and track length histograms (corrected lengths) for confined track measurements from samples X6, X7, 2495-3, and 2495-1 using the HeFTy software of *Ketcham* [2005]. See text for discussion. Initiation of more rapid Cenozoic cooling occurs after 40 Ma. The sample is constrained to at- or near-surface temperatures at the time of sedimentary deposition (box labeled D), and at the present day, but we have allowed the model a large degree of freedom in choosing the cooling and burial path between these surface constraint points (large black boxes). Details of modeling options used are outlined in methods section. The dark grey field in each model shows the envelope of possible good fit paths and the light grey field shows the envelope of possible acceptable fit paths, defined by merit values of 0.5 and 0.05, respectively. MTL is the C-axis corrected mean track length (error 1-sigma). Age is the central age in Ma, with 2-sigma errors.

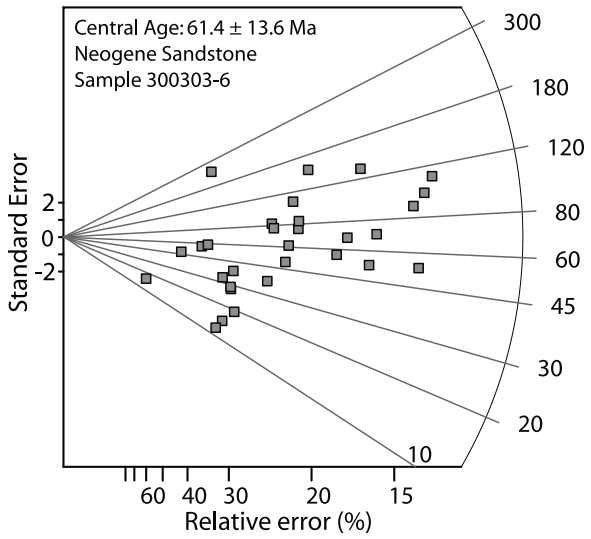

Figure 11. Radial plot for apatite grains from Neogene sand sample 300303-6.

[49] Subsequently, the transition to an erosive regime led to the situation where Cretaceous (and Eocene) strata now only crop out on the westernmost boundaries of the Sichuan Basin, with a corresponding reduction in stratigraphic thickness toward the present-day fluvial exit of the basin at the Three Gorges (Figure 3d). It is clear that much of this younger stratigraphy has been eroded over a large proportion of the Sichuan Basin, such that progressively older strata crop out toward the east (Figure 1), with the current basin surface being an erosional horizon. Only to the west of the Longquan Anticline is this erosional surface represented as an unconformity, between Neogene and Quaternary strata and the subcropping Eocene, Cretaceous and, to a lesser extent, Jurassic and Triassic strata. The Neogene and Quaternary sediments owe their presence in the Chengdu subbasin to the Longquan Anticline [*Burchfiel et al.*, 1995], which acts as a sediment dam. The remainder of the Sichuan Basin continued to be erosional into modern times, as evidenced by the lack of Quaternary deposits.

6.2. Mechanisms for Basin Erosion

[50] The mechanism by which such a large quantity of sedimentary rock could have been removed from the basin almost certainly involves the Yangtze River and its tributaries. The present-day Yangtze River clearly has enormous capacity to transport sediment, with measured mean sediment loads of 527.2 Mt a^{-1} at the eastern exit of the Three Gorges (Yichang) between 1950 and 1986, before closure of the Three Gorges dam [*Higgitt and Lu*, 2001; *Xu et al.*, 2006]. This is equivalent to removal of a 2 km thick layer of sedimentary rock over the ~225,000 km^2 surface area of the basin within approximately 2 Ma (assuming a bulk rock density of 2200 kg m^{-2}). It seems equally clear that the transition from sedimentologically closed basin conditions in the Mesozoic to the present throughgoing Yangtze River system must have involved significant drainage reorganization at some point in the Cenozoic. This drainage reorganization was most likely accompanied by a lowering of base level, leading to the initiation of erosion of the basin fill. Whilst the triggers of, and the processes leading to, such continent-scale drainage changes are not fully understood, physiographic and geologic evidence allows us to consider possible theoretical mechanisms for this reorganization.

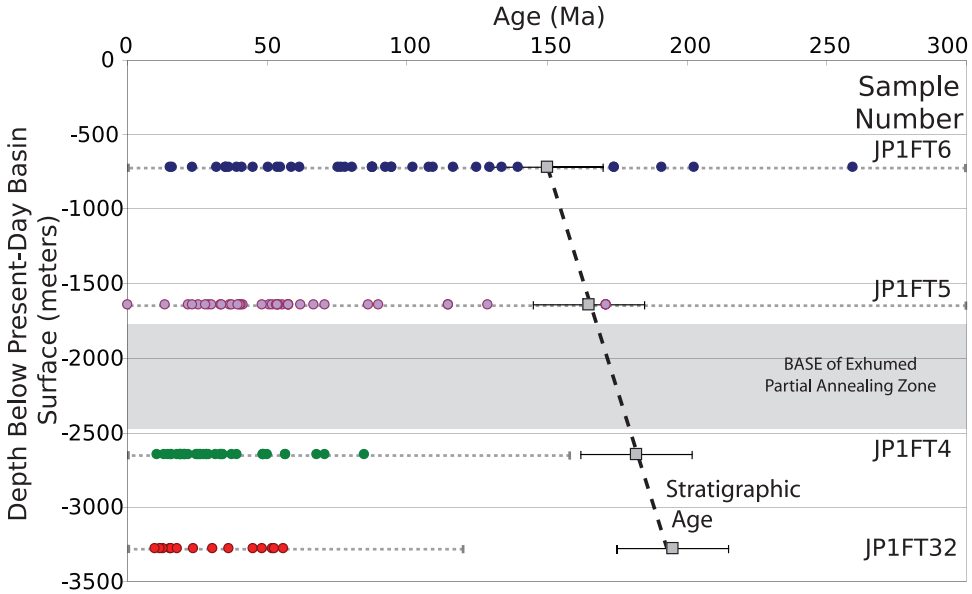

Figure 12. Single-grain apatite fission track ages (circles) for samples in Borehole JP1 (Figure 6) plotted against drilled depth below the present day topographic surface. Squares and thick dashed line show the stratigraphic age of each sample. Single grain ages decrease downsection, reflecting the increasing degree of fission track resetting with depth. Two-sigma error bars for single grain ages are shown by thin dashed lines. Errors in the stratigraphic ages are assumed to be ±20 Ma and are shown by solid black error bars.

[51] The first of these mechanisms, proposed by *Barbour* [1936] and further developed by *Clark et al.* [2004], involves a Middle Yangtze River draining to the southwest that was initially distinct from the eastward draining Lower Yangtze River. *Clark et al.* [2004] postulated that the original drainage divide between the Lower and Middle Yangtze lay at the present position of the Three Gorges. In this model, all the major rivers of the eastern Tibetan Plateau initially drained generally southward into the South China Sea. The flow of the Middle Yangtze River was ''reversed'' through gradual headward erosion by the Lower Yangtze River through the Three Gorges region, resulting in a major peturbation to the entire East Asian fluvial system. Successive river captures then occurred from east to west, progressively integrating more westerly rivers into the catchment of the growing Yangtze River as headward erosion progressed [*Clark et al.*, 2004]. Presumably, the adjustment of the Sichuan Basin area to a new base level set by the Lower Yangtze in the east would have been accompanied by an extensive change in erosion patterns.

[52] An alternative but equally feasible model involves the transition from internal to external drainage within Sichuan Basin itself. Rather than initial headward erosion as the cause, we suggest that filling and spilling of the basin's contents through the site of the Three Gorges may have led to linkage with the Lower Yangtze and rapid incision at the basin's new outlet. If the Sichuan Basin was accumulating sediment through the Mesozoic and into Paleogene time, it probably became topographically elevated relative to the subsiding, extensional Jianghan and Dongting Basins to the east [*Ulmishek*, 1992]. Filling of the basin would inevitably have progressed to a critical level where spilling of either the sedimentary fill or an associated lake resulted in breaching of the topographic barrier at the eastern boundary of the basin. This would have led to a sudden increase in discharge at the new drainage exit of the basin, resulting not only in incision through the former barrier but also an increase in discharge to the east of this point into the Lower Yangtze. Consequently, a knickpoint would have migrated headward into the Sichuan Basin, resulting in erosion of the basin's sedimentary fill. This headward migration would likely have caused capture and diversion of drainage within the Sichuan Basin; in other words, these two mechanisms are not mutually exclusive, and it seems probable that some combination was responsible for the large-scale redirection of the Middle Yangtze through the Three Gorges and into the Lower Yangtze. Although we cannot distinguish between the two mechanisms with our data, note that the end result in both scenarios is the same, integration of the Sichuan Basin into the Yangtze River drainage basin and erosion within the basin in response to lowered base level.

[53] Such fill and spill processes are a well-documented occurrence in sedimentary basins in a variety of environmental settings and on a variety of scales [e.g., *Einsele and Hinderer*, 1997; *Sinclair and Tomasso*, 2002; *Sobel et al.*, 2003]. A notable example is the Ebro Basin of northeastern Spain, which was internally drained from ca. 40 Ma to 11.5 Ma, when the Catalan Coastal Range was breached by the Ebro River and the predominantly lacustrine sediments of the previously enclosed basin were eroded into the Valencia Trough [*Garcia-Castellanos et al.*, 2003]. Examples also exist of internally drained basins which may at a future stage become incorporated into an external drainage network, particularly the Tarim and Qaidam Basins in Northern Tibet. Passages from internally to externally drained conditions have also been linked with changes from dryer to wetter climates [*Sobel et al.*, 2003].

6.3. Implications for the Eastern Tibetan Plateau and Three Gorges Regions

[54] The contrast in erodability of the strata within the Sichuan Basin compared to the lithologies exposed in one of the adjacent orogens, the Longmen Shan, would also have led to a contrast in erosion across this mountain front. Higher erosion rates in the Sichuan Basin would have resulted in more rapid lowering of the basin, thereby increasing the relief across this margin without any need for crustal shortening or lower-crustal flow. As a consequence, focused erosion along the Longmen Shan could also be expected, whether or not a high plateau margin had been established in Eastern Tibet at this time. For these reasons, it is dangerous to correlate geomorphic surfaces across the margin. Our research suggests that there is a discrepancy in the timing of the initiation of enhanced exhumation in the Longmen Shan (<12 Ma) [*Arne et al.* 1997, *Kirby et al.*, 2002] and that within the Sichuan Basin (<40 Ma). This could possibly be explained by (1) focused cooling along the mountain front, which is only detectable through detailed sampling for low-temperature thermochronology, or, more probably, (2) the older event may only be observed in the cooling history of higher temperature thermochronometers (e.g., zircon fission track), since the AFT paleo-PAZ for this event has probably already been eroded along the eastern margin of the Tibetan Plateau [*Xu and Kamp*, 2000; *Kirby et al.*, 2002].

[55] An explanation as to why the Yangtze exits the Sichuan Basin in the east may be because it represented the lowest topographic point in any of the barriers around the basin at the time. Although the Yangtze River exhibits some characteristics typical of antecedence within the basin, such as cutting across anticlines [*Simpson*, 2004], in the majority of locations it is controlled by tectonic structures, flowing parallel to strike. Certainly, the convergence of the major southwest-northeast structural trends of the Hunan-Guangxi fold belt and the northwest-southeast structural trends of the Daba Shan fold and thrust belt to form the primarily east-west trends of the Three Gorges region (Figure 1) must have been a first-order control and may have led to the subsequent ''funneling'' of drainage channels along this trend.

[56] If cooling of strata within the Sichuan Basin was indeed initiated by the formation of a major drainage route through the Three Gorges region, then such an event should also be chronicled by the initiation of erosion and rapid cooling within the Gorges themselves. We would expect that the age of this cooling event would be equivalent to, or slightly older than, the <40 Ma event that is exhibited by our apatite fission track data within the basin. Previous attempts to provide time constraints on the cutting of the Three Gorges have only provided dates on terrace deposits at the western end of the gorges using techniques that do not have the range to date back to the Early-Middle Tertiary

[e.g., *Li et al.*, 2001]. A more promising avenue of future research may be the sedimentary record of gorge incision and basin denudation within onshore and offshore basins that lie downstream of the Three Gorges. A critical test of our hypothesis would involve an integrated sedimentary study (geochronology, sediment budgets, geochemical provenance, etc.) of basins downstream from the Jianghan Basin, immediately east of the Three Gorges, down to the East China Sea. The removal of so much mass from the lithosphere may also mean that there are other, detectable far-field tectonic implications due to unloading.

[57] In summary, we propose that the initial establishment of the Yangtze River through the Three Gorges was the most likely trigger of increased erosion rates within the Sichuan Basin and its hinterland regions. The basin response to this reorganization involved stripping of highly erodable basin sediments as a result of knickpoint propagation headward from the newly established gorge into the previously sedimentologically enclosed (if not hydrologically enclosed) basin. The lowering of base level within the basin by >2 km also resulted in enhanced erosion rates in the river valleys of the surrounding orogens and renewed headward propagation within the corresponding drainages. The perturbation to the fluvial network resulting from incision of the Three Gorges may have been the trigger for subsequent drainage captures. The most notable capture event of this type within the Yangtze drainage basin is that of the Upper Yangtze from the Red River by the Middle Yangtze [*Clark et al.*, 2004] and this is reflected in the offshore clastic sedimentary record [*Clift*, 2006]. Recent results from the Yinggehai-Song Hong Basin, Gulf of Tonkin in the Red River offshore region indicate a significant change in the εNd values of the sediment toward the end of the Eocene, perhaps reflecting this capture event [*Clift and Sun*, 2006, X. Clift, personal communication, 2004]. Thus the Middle and Lower Yangtze domains must have already been integrated by this time. This is in agreement with the timing of cooling interpreted as erosional events from our new data set.

7. Conclusions

[58] The Sichuan Basin is located immediately to the east of the Tibetan Plateau, in a strategically important location for assessing tectonic models of plateau formation and studying major drainage changes that occurred on the Asian continent during the Cenozoic. Apatite fission track analysis of detrital sediments within the Sichuan Basin reveals that a paleopartial annealing zone is exposed over a large area of the Sichuan Basin, indicating widespread exhumation of the basin following a long period of Late Triassic to Eocene continental deposition. Apatite fission track stratigraphic-age profiles, combined with thermal history modeling of the samples, allow us to constrain the initiation of the related cooling event to some time after 40 Ma. Additionally, we can put bounds on the thickness of sedimentary material that was removed from the basin at between 1.3 and 4 km.

[59] The remaining Mesozoic stratigraphy within the Sichuan Basin indicates that until at least the Late Cretaceous, the basin was internally drained and enclosed on all sides by mountains. Since the basin is now drained by the Yangtze River and a number of major tributaries, the transition from internal to external drainage must have occurred during the Cenozoic, and this reorganization was the likely trigger for large-magnitude erosion within the basin indicated by the fission track data. We hypothesize that the stimulus for this event was the integration of the Middle Yangtze and Lower Yangtze Rivers through the Three Gorges area, resulting in increased erosion rates that propagated headward through the Sichuan Basin and in subsequent capture events to the west. The knock-on effects of this event may have included an increase in relief at the margins of the basin, including the Longmen Shan; gorge incision; and major drainage reorganizations that occurred throughout Southeast Asia.

[60] **Acknowledgments.** This research was supported financially by ETH Zurich Research Commission grant TH-4/03-01 and US NSF grant EAR-0125565. The authors gratefully acknowledge a financial contribution from Shell that enabled the publication of this research. We thank the Chengdu University of Technology and their members for essential support and extend particular gratitude to Cristina Keller, Damian Steffen, and Li Bing for their assistance in the field and to Wang Mo for organizational help. Philip Allen, Dennis Arne, Eva Enkelmann, Liu Shugen, Guy Simpson, and Ed Sobel are thanked for useful discussions. Andrew Gleadow and Eric Kirby are thanked for their helpful reviews. We also appreciate an extra, independent review by Chris Wilson and his efforts in facilitating contact between Zurich and Melbourne. Requests for additional data and materials should be directed to N.J. Richardson (nicholas.richardson@shell.com).

References

Allen, P. A., and J. R. Allen (1990), *Basin Analysis: Principles and Applications*, Blackwell Sci., Oxford, U. K.

Arne, D., B. Worley, C. Wilson, S. Chen, D. Foster, Z. Luo, S. Liu, and P. Dirks (1997), Differential exhumation in response to episodic thrusting along the eastern margin of the Tibetan Plateau, *Tectonophysics*, *280*, 239–256.

Barbour, G. B. (1936), Physiographic History of the Yangtze, *Geogr. J.*, *87*(1), 17–34.

Burchfiel, B. C., Z. Chen, Y. Liu, and L. H. Royden (1995), Tectonics of the Longmen Shan and adjacent regions, *Int. Geol. Rev.*, *37*, 661–735.

Burtner, R. L., A. Nigrini, and R. A. Donelick (1994), Thermochronology of lower Cretaceous source rocks in the Idaho-Wyoming thrust belt, *Am. Assoc. Petrol. Geol. Bull.*, *78*(10), 1613–1636.

Cai, L., and H. Liu (1996), Evolution of foreland basins on the borders of the Yangtze block, *Earth Sci. J. Chin. Univ. Geosci.*, *21*, 433–440.

Chen, S. F., and C. J. L. Wilson (1996), Emplacement of the Longmen Shan Thrust-Nappe Belt along the eastern margin of the Tibetan Plateau, *J. Struct. Geol.*, *18*, 413–430.

Chen, S. F., C. J. L. Wilson, Q. D. Deng, X. L. Zhao, and Z. L. Luo (1994), Active faulting and block movement associated with large earthquakes in the Min Shan and Longmen Mountains, northeastern Tibetan Plateau, *J. Geophys. Res.*, *99*(B12), 24,025–24,038.

Chen, S. F., C. J. L. Wilson, and B. A. Worley (1995), Tectonic transition from the Songpan-Garze fold belt to the Sichuan Basin, southwestern China, *Basin Res.*, *7*, 235–253.

Chen, Z., B. C. Burchfiel, Y. Liu, R. W. King, L. H. Royden, W. Tang, E. Wang, J. Zhao, and X. Zhang (2000), Global Positioning System measurements from eastern Tibet and their implications for India/Eurasia intercontinental deformation, *J. Geophys. Res.*, *105*(B7), 16,215–16,228.

Clark, M. K., and L. H. Royden (2000), Topographic ooze: Building the eastern margin of Tibet by lower crustal flow, *Geology*, *28*(8), 703–706.

Clark, M. K., L. M. Schoenbohm, L. H. Royden, K. X. Whipple, B. C. Burchfiel, X. Zhang, W. Tang, E. Wang, and L. Chen (2004), Surface uplift, tectonics, and erosion of eastern Tibet from large-scale drainage patterns, *Tectonics*, *23*, TC1006, doi:10.1029/2002TC001402.

Clark, M. K., M. A. House, L. H. Royden, K. X. Whipple, B. C. Burchfiel, X. Zhang, and W. Tang (2005), Late Cenozoic uplift of southeastern Tibet, *Geology*, *33*, 525–528.

Clift, P. D. (2006), Controls on the erosion of Cenozoic Asia and the flux of clastic sediment to the ocean, *Earth Planet. Sci. Lett.*, *241*, 571–580, doi:10.1016/j.epsl.2005.11.028.

Clift, P. D., and Z. Sun (2006), The sedimentary and tectonic evolution of the Yinggehai-Song Hong Basin and the southern Hainan margin, South

China Sea: Implications for Tibetan uplift and monsoon intensification, *J. Geophys. Res.*, *111*, B06405, doi:10.1029/2005JB004048.

Clift, P. D., J. Blusztajn, and N. A. Duc (2006), Large-scale drainage capture and surface uplift in eastern Tibet-SW China before 24 Ma inferred from sediments of the Hanoi Basin, Vietnam, *Geophys. Res. Lett.*, *33*, L19403, doi:10.1029/2006GL027772.

Co-Operative Geological Group of Japan and China in the Panxi Region (1986), Geology of the Panxi region, Sichuan Province, southwest China: Report of the 1983–1984 co-operative research of Japan and China, 340 pp., Yamaguchi Univ., Yoshida, Japan.

Corrigan, J. D. (1993), Apatite fission-track analysis of Oligocene strata in South Texas, U.S.A., *Chem. Geol.*, *104*, 227–249.

Densmore, A. L., M. A. Ellis, Y. Li, R. Zhou, G. S. Hancock, and N. J. Richardson (2007), Active tectonics of the Beichuan and Pengguan faults at the eastern margin of the Tibetan Plateau, *Tectonics*, *26*, TC4005, doi:10.1029/2006TC001987.

Dirks, P. H., C. J. L. Wilson, S. Chen, Z. Luo, and S. Liu (1994), Tectonic evolution of the NE margin of the Tibetan Plateau: Evidence from the central Longmen Mountain, Sichuan Province, *China, J. Southeast Asian Earth Sci.*, *9*, 181–192.

Dumitru, T. A. (1995), A new computer automated microscope stage system for fission track analysis, *Nucl. Tracks Radiat. Meas.*, *21*, 575–580.

Einsele, G., and M. Hinderer (1997), Terrestrial sediment yield and the lifetimes of reservoirs, lakes and larger basins, *Geol. Rundsch.*, *86*, 288–310.

England, P. C., and G. A. Houseman (1986), Finite strain calculations of continental deformation: 2. Comparison with the India-Asia collision zone, *J. Geophys. Res.*, *91*(B3), 3664–3676.

England, P. C., and P. Molnar (1990), Right-lateral shear and rotation as the explanation for strike-slip faulting in eastern Tibet, *Nature*, *344*, 140–142, doi:10.1038/344140a0.

Enkelmann, E., L. Ratschbacher, and R. Jonckheere (2004), Cenozoic tectonics of the easternmost Tibetan Plateau: Constraints from fission-track thermochronology, paper presented at 10th International Conference on Fission Track Dating and Thermochronology, Amsterdam.

Enkelmann, E., L. Ratschbacher, R. Jonckheere, R. Nestler, M. Fleischer, R. Gloaguen, B. R. Hacker, Y. Q. Zhang, and Y. S. Ma (2006), Cenozoic exhumation and deformation of northeastern Tibet and the Qinling: Is Tibetan lower crustal flow diverging around the Sichuan Basin?, *Geol. Soc. Am. Bull.*, *118*(5), 651–671.

Enkin, R., V. Courtillot, L. Xing, Z. Zhang, Z. Zhuang, and J. Zhang (1991a), The stationary Cretaceous paleomagnetic pole of Sichuan (South China Block), *Tectonics*, *10*, 547–559.

Enkin, R., Y. Chen, V. Courtillot, J. Besse, L. Xing, Z. Zhang, Z. Zhuang, and J. Zhang (1991b), A Cretaceous pole from south China and the Mesozoic hairpin turn of the Eurasian apparent polar wander path, *J. Geophys. Res.*, *96*, 4007–4027.

Farley, K. A. (2000), Helium diffusion from apatite; general behavior as illustrated by Durango fluorapatite, *J. Geophys. Res.*, *105*(B2), 2903–2914.

Farley, K. A., and L. T. Silver (1996), The effects of long alpha-stopping distances on (U-Th)/He ages, *Geochim. Cosmochim. Acta*, *60*(21), 4223–4229.

Fitzgerald, P. G., S. L. Baldwin, and L. E. Webb (2006), Interpretation of (U-Th)/He single grain ages from slowly cooled crustal terranes: A case study from the Transantarctic Mountains of southern Victoria Land, *Chem. Geol.*, *225*, 91–120.

Galbraith, R. (1981), On statistical models for fission track counts, *Math. Geol.*, *13*, 471–488.

Galbraith, R. F., and G. M. Laslett (1993), Statistical models for mixed fission-track ages, *Nucl. Tracks Radiat. Meas.*, *21*, 459–470.

Garcia-Castellanos, D., J. Vergés, J. M. Gaspar-Escribano, and S. Cloetingh (2003), Interplay between tectonics, climate and fluvial transport during the Cenozoic evolution of the Ebro Basin (NE Iberia), *J. Geophys. Res.*, *108*(B7), 2347. doi:10.1029/2002JB002073.

Gilder, S., and V. Courtillot (1997), Timing of the north-South China collision from new middle to late Mesozoic paleomagnetic data from the North China Block, *J. Geophys. Res.*, *102*(B8), 17,713–17,727.

Gleadow, A. J. W., and I. Duddy (1981), A natural long term annealing experiment for apatite, *Nucl. Tracks Radiat. Meas.*, *5*, 169–174.

Harrowfield, M. J., and C. J. L. Wilson (2005), Indosinian deformation of the Songpan Garzê Fold Belt, northeast Tibetan Plateau, *J. Struct. Geol.*, *27*, 101–117.

Hearn, T. M., S. Wang, J. F. Ni, Z. Xu, Y. Yu, and X. Zhang (2004), Uppermost mantle velocities beneath China and surrounding regions, *J. Geophys. Res.*, *109*, B11301, doi:10.1029/2003JB002874.

Hearn, T. M., S. Wang, S. Pei, J. F. Ni, X. Zhonghai, and Y. Yu (2005), Short-period surface-wave amplitude tomography of China, *Eos Trans. AGU*, *86*(52), Fall Meet. Suppl., Abstract T41A-1274.

Higgitt, D. L., and X. X. Lu (2001), Sediment delivery to the three gorges: 1. Catchment controls, *Geomorphology*, *41*, 143–156.

Hsü, K. J. (1989), Origin of Sedimentary Basins of China, in *Chinese Sedimentary Basins,* vol. 1, *Sedimentary Basins of the World*, edited by X. Zhu, pp. 147–163, Elsevier, Amsterdam.

Hsü, K. J., J. Li, H. Chen, Q. Wang, S. Sun, and A. M. C. Sengor (1990), Tectonics of South China: Key to understanding West Pacific geology, *Tectonophysics*, *183*, 9–39.

Hu, S., L. He, and J. Wang (2000), Heat flow in the continental area of China: A new data set, *Earth Planet. Sci. Lett.*, *179*(2), 407–419.

Huang, K., and N. D. Opdyke (1991), Paleomagnetism of Jurassic rocks from southwestern Sichuan and the timing of the closure of the Qinling Suture, *Tectonophysics*, *200*, 299–316.

Hurford, A. J., and P. F. Green (1983), The zeta age calibration of fission-track dating, *Chem. Geol.*, *41*, 285–317.

Ketcham, R. A. (2003), Observations on the relationship between crystallographic orientation and biasing in apatite fission-track measurements, *Am. Mineral.*, *88*, 817–829.

Ketcham, R. A. (2005), Forward and inverse modeling of low-temperature thermochronometry data, in *Low-Temperature Thermochronology: Techniques, Interpretations, and Applications,* vol. 58, *Reviews in Mineralogy and Geochemistry,* edited by P. W. Reiners and T. A. Ehlers, pp. 275–314, Mineral. Soc. of Am., Chantilly, Va.

Ketcham, R. A., R. A. Donelick, and W. D. Carlson (1999), Variability of apatite fission-track annealing kinetics III: Extrapolation to geological time scales, *Am. Mineral.*, *84*, 1235–1255.

Kimura, G., M. Takahasho, and M. Kono (1990), Mesozoic collision-extrusion tectonics in eastern Asia, *Tectonophysics*, *181*, 15–23.

Kirby, E., K. X. Whipple, B. C. Burchfiel, W. Tang, G. Berger, and Z. Sun (2000), Neotectonics of the Min Shan, China: Implications for mechanisms driving Quaternary deformation along the eastern margin of the Tibetan Plateau, *Geol. Soc. Am. Bull.*, *112*(3), 375–393.

Kirby, E., P. Reiners, M. Krol, K. Hodges, K. Whipple, K. Farley, W. Tang, and Z. Chen (2002), Late Cenozoic uplift and landscape evolution along the eastern margin of the Tibetan Plateau: Inferences from $^{40}Ar/^{39}Ar$ and (U-Th)/He thermochronology, *Tectonics*, *21*(1), 1001, doi:10.1029/2000TC001246.

Kirby, E., K. X. Whipple, W. Tang, and Z. Chen (2003), Distribution of active rock uplift along the eastern margin of the Tibetan Plateau: Inferences from bedrock channel longitudinal profiles, *J. Geophys. Res.*, *108*(B4), 2217, doi:10.1029/2001JB000861.

Korsch, R. J., H. Z. Mai, Z. C. Sun, and J. D. Gorter (1997), Evolution and subsidence history of the Sichuan Basin, Southwest China, in *Basin Analysis, Global Sedimentary Geology and Sedimentology*, vol. 8, *Proceedings of the 30th International Geological Congress, China*, edited by B. J. Liu and S. T. Li, pp. 208–221, VSP, Utrecht, Netherlands.

Laslett, G. M., P. F. Green, I. R. Duddy, and A. J. W. Gleadow (1987), Thermal annealing of fission tracks in apatite: 2, A quantitative analysis, *Chem. Geol.*, *65*, 1–13.

Li, J., S. Xie, and M. Kuang (2001), Geomorphic evolution of the Yangtze Gorges and the time of their formation, *Geomorphology*, *41*, 125–135.

Li, Y., P. A. Allen, A. L. Densmore, and X. Qiang (2003), Evolution of the Longmen Shan Foreland Basin (western Sichuan, China) during the Late Triassic Indosinian Orogeny, *Basin Res.*, *15*, 117–138.

Liang, C., X. Song, and J. Huang (2004), Tomographic inversion of Pn travel times in China, *J. Geophys. Res.*, *109*, B11304, doi:10.1029/2003JB002789.

Liu, B., and Y. Zheng (1988), *Mesozoic Sedimentary Facies of the Southern Sichuan Basin*. IAS Excursion Guide Book B4, IAS International Symposium on Sedimentology Related to Mineral Deposits, Beijing, China.

Liu, X., P. Zhou, Z. Xia, C. Yuan, R. Li, M. Wang, and L. Zeng (1982), *Continental Mesozoic Stratigraphy and Paleontology in Sichuan Basin of China* (in Chinese), People's Publ. House of Sichuan, Chengdu, China.

Ma, L., X. Qiao, L. Min, B. Fan, X. Ding, and N. Liu (2002), *Geological Atlas of China*, Geol. Publ. House, Beijing.

Mattauer, M., P. Matte, J. Malavieille, P. Tapponnier, H. Maluski, Z. Q. Xu, Y. L. Lu, and Y. Q. Tang (1985), Tectonics of the Qinling Belt: build-up and evolution of eastern Asia, *Nature*, *317*, 496–500.

Meng, Q. R., and G. W. Zhang (1999), Timing of the collision of the North and South China Blocks: Controversy and reconciliation, *Geology*, *27*, 123–126.

Meng, Q.-R., E. Wang, and J.-M. Hu (2005), Mesozoic sedimentary evolution of the northwest Sichuan basin: Implication for continued clockwise rotation of the South China block, *Geol. Soc. Am. Bull.*, *117*, 396–410.

Molnar, P., and P. Tapponnier (1975), Cenozoic Tectonics of Asia: Effects of a continental collision, *Science*, *189*(4201), 419–426.

O'Sullivan, P. B., and R. R. Parrish (1995), The importance of apatite composition and single-grain ages when interpreting fission track data

from plutonic rocks: A case study from the Coast Ranges, British Columbia, *Earth Planet. Sci. Lett.*, *132*, 213–224.
Petroleum Geology of China (1987), *Sichuan Oil and Gas Field*, vol. 10, 250 pp., Beijing.
Regional Geology of Sichuan Province (1991), *People*'s *Republic of China Ministry of Geology and Mineral Resources*, Ser. 1, vol. 23, 730 pp., Geol. Publ. House, Beijing.
Ratschbacher, L., B. R. Hacker, A. Calvertc, L. E. Webb, J. C. Grimmer, M. O. McWilliams, T. Ireland, S. Dong, and J. Hu (2003), Tectonics of the Qinling (Central China): Tectonostratigraphy, geochronology, and deformation history, *Tectonophysics*, *366*, 1–53.
Royden, L. H., B. C. Burchfiel, R. W. King, E. Wang, Z. Chen, F. Shen, and Y. Liu (1997), Surface deformation and lower crustal flow in eastern Tibet, *Science*, *276*, 788–790.
Ruiz, G. M. H., D. Seward, and W. Winkler (2004), Detrital thermochronology-A new perspective on hinterland tectonics, an example from the Andean Amazon Basin, Ecuador, *Basin Res.*, *16*(3), 413, doi:10.1111/j.1365-2117.2004.00239.
Schoenbohm, L. M., K. X. Whipple, B. C. Burchfiel, and L. Chen (2004), Geomorphic constraints on surface uplift, exhumation, and plateau growth in the Red River region, Yunnan Province, China, *Geol. Soc. Am. Bull.*, *116*(7-8), 895–909.
Seward, D. (1989), Cenozoic basin histories determined by fission-track dating of basement granites, South Island, New Zealand, *Chem. Geol.*, *79*(11), 31–48.
Seward, D., R. Spikings, G. Viola, A. Kounov, G. Ruiz, and N. Naeser (2000), Etch times and operator variation for spontaneous track length measurements in apatites: An intra-laboratory check, *On Track*, *10*, 19–21.
Schegg, R., and W. Leu (1998), Analysis of erosion events and paleogeothermal gradients in the North Alpine Foreland Basin of Switzerland, in Basin Modelling: Practice and Progress, edited by S. Duppenbecker and J. E. Illife, *Geol. Soc. Spec. Publ.*, *141*, 137–155.
Simpson, G. (2004), Role of river incision in enhancing deformation, *Geology*, *32*(4), 341–344.
Sinclair, H. D., and M. Tomasso (2002), Depositional Evolution of Confined Turbidite Basins, *J. Sediment. Res.*, *72*(4), doi:10.1306/111501720451.
Sobel, E. R., G. E. Hilley, and M. R. Strecker (2003), Formation of internally drained contractional basins by aridity-limited bedrock incision, *J. Geophys. Res.*, *108*(B7), 2344, doi:10.1029/2002JB001883.
Tapponnier, P., G. Peltzer, A. Y. Le Dain, R. Armijo, and P. Cobbold (1982), Propagating extrusion tectonics in Asia: New insights from simple experiments with plasticine, *Geology*, *10*(12), 611–616.
Ulmishek, G. (1992), Geology and hydrocarbon resources of onshore basins in eastern China, *U.S. Geol. Surv. Open File Rep.*, *93–4*.
Vermeesch, P. (2004), How many grains are needed for a provenance study?, *Earth Planet. Sci. Lett.*, *224*(3–4), 441–451.
Wallis, S., T. Tsujimori, M. Aoya, T. Kawakami, K. Terada, K. Suzuki, and H. Hyodo (2003), Cenozoic and Mesozoic metamorphism in the Longmenshan orogen: Implications for geodynamic models of eastern Tibet, *Geology*, *31*, 745–748.
Wan, T., and H. Zhu (1991), Tectonic events of Late Proterozoic-Triassic in South China, *J. Southeast Asian Earth Sci.*, *6*, 147–157.
Wang, E., B. C. Burchfiel, L. H. Royden, L. Chen, J. Chen, W. Li, and Z. Chen (1998), Late Cenozoic Xianshuihe-Xiaojiang, Red River and Dali fault systems of southwestern Sichuan and central Yunnan, China, *Geol. Soc. Am. Spec. Pap.*, *327*, 108 pp.
Wang, E., Q. Meng, B. C. Burchfiel, and G. Zhang (2003), Mesozoic large-scale lateral extrusion, rotation and uplift of the Tongbai-Dabie Shan belt in east China, *Geology*, *31*(4), 307–310.
Wang, J., C. Bao, Z. Lou, and Z. Guo (1989), Formation and Development of the Sichuan Basin, in *Chinese Sedimentary Basins*, vol. 1, *Sedimentary Basins of the World,* edited by X. Zhu., pp. 147–163, Elsevier, Amsterdam.
Wang, S., T. M. Hearn, S. Pei, Z. Xu, and J. F. Ni (2005), Amplitude tomography from ML-magnitude data beneath China, *Eos Trans. AGU*, *86*(52), Fall Meet. Suppl., Abstract T41A-1273.
Weislogel, A. L., S. A. Graham, E. Z. Chang, J. L. Wooden, G. E. Gehrels, and H. Yang (2006), Detrital zircon provenance of the Late Triassic Songpan-Ganzi complex: Sedimentary record of collision of the North and South China blocks, *Geology*, *34*, 97–100.
Wilson, C. J. L., M. J. Harrowfield, and A. J. Reid (2006), Brittle modification of Triassic architecture in eastern Tibet: implications for the construction of the Cenozoic plateau, *J. Asian Earth Sci.*, *27*(3), 341–357.
Wipf, M. A. (2006), Evolution of the Western Cordillera and coastal margin of Peru: Evidence from low-temperature thermochronology and geomorphology, dissertation, Naturwissenschaften, ETH Zürich, Zürich. (Available at http://e-collection.ethbib.ethz.ch/show?type=diss&nr=16383)
Wolf, R. A., K. A. Farley, and L. T. Silver (1996), Helium diffusion and low-temperature thermochronometry of apatite, *Geochim. Cosmochim. Acta*, *60*(21), 4231–4240.
Wu, D., and N. Wu (1998), Paleotemperature of the Sichuan Basin and its geological significance, *Acta Petrol. Sin.*, *19*(1), 18–23.
Xie, X., and H. Yu (1988), Geothermal character of Sichuan Basin (in Chinese), *J. Chengdu Coll. Geol.*, *15*, 107–112.
Xu, G. (1997), Thermo-tectonic history of eastern Tibetan Plateau and western Sichuan Basin, China, assessed by fission track thermochronology, Ph.D. thesis, 353 pp., Univ. of Waikato, Hamilton, New Zealand.
Xu, G., and P. J. J. Kamp (2000), Tectonics and denudation adjacent to the Xianshuihe Fault, eastern Tibetan Plateau: Constraints from fission track thermochronology, *J. Geophys. Res.*, *105*(B8), 19,231–19,251.
Xu, K., J. D. Milliman, Z. Yang, and H. Wang (2006), Yangtze sediment decline partly from Three Gorges Dam, *Eos Trans. AGU*, *87*(19), 185.
Yan, D., M. Zhou, H. Song, X. Wang, and M. Malpas (2003), Origin and tectonic significance of a Mesozoic multi-layer over-thrust system within the Yangtze Block (South China), *Tectonophysics*, *361*, 239–254, doi:10.1016/S0040-1951(02)00646-7.
Yang, Z., Y. Chang, and H. Wang (1986), *Geology of China*, 303 pp., Oxford Univ. Press, Oxford, U. K.
Yokoyama, M., Y. Liu, N. Halim, and Y. Otofuji (2001), Paleomagnetic study of Upper Jurassic rocks from the Sichuan basin: tectonic aspects for the collision between the Yangtze Block and the North China Block, *Earth Planet. Sci. Lett.*, *193*(3–4), 273–285.
Zhang, K. J. (1997), North and South China collision along the eastern and southern North China margins, *Tectonophysics*, *270*, 145–156.
Zhang, P. Z., et al. (2004), Continuous deformation of the Tibetan Plateau from global positioning system data, *Geology*, *32*(9), 809–812, doi:10.1130/G20554.1.
Zhang, Y., Y. Luo, and C. Yang (1990), *Panxi Rift and its Geodynamics*, 415 pp., Geol. Publ. House, Beijing, China.
Zhao, X., and R. S. Coe (1987), Palaeomagnetic constraints on the collision and rotation of North and South China, *Nature*, *327*, 141–144, doi:10.1038/327141a0.
Zheng, J., W. L. Griffin, S. Y. O'Reilly, M. Zhang, N. Pearson, and Y. Pan (2006), Widespread Archean basement beneath the Yangtze craton, *Geology*, *34*(6), 417–420.

A. L. Densmore, Department of Geography, Durham University, South Road, Durham, DH1 3LE, UK. (a.l.densmore@durham.ac.uk)
M. A. Ellis, Center for Earthquake Research and Information, University of Memphis, Memphis, TN 38152, USA.
A. Fowler, AGD Operations, RSD 4220, Heathcote, VIC 3523, Australia.
N. J. Richardson, Shell UK Limited, 1 Altens Farm Road, Nigg, Aberdeen AB12 3FY, UK. (nicholas.richardson@shell.com)
D. Seward, Department of Earth Sciences, Institute of Geology, ETH Zürich, CH-8092 Zürich, Switzerland.
M. Wipf, Geologisch-Paläontologisches Institut, Im Neuenheimer Feld 234, D-69120 Heidelberg, Germany. (martinwipf@hotmail.com)
L. Yong and Y. Zhang, National Key Laboratory of Oil and Gas Reservoir Geology and Exploration, Chengdu University of Technology, Chengdu 610059, Sichuan, China.